National Library of Canada
Bibliothèque nationale du Canada

Canadian Theses Service
Service des thèses canadiennes

Ottawa, Canada
K1A 0N4

NOTICE

The quality of this microform is heavily dependent upon the quality of the original thesis submitted for microfilming. Every effort has been made to ensure the highest quality of reproduction possible.

If pages are missing, contact the university which granted the degree.

Some pages may have indistinct print especially if the original pages were typed with a poor typewriter ribbon or if the university sent us an inferior photocopy.

Reproduction in full or in part of this microform is governed by the Canadian Copyright Act, R.S.C. 1970, c. C-30, and subsequent amendments.

AVIS

La qualité de cette microforme dépend grandement de la qualité de la thèse soumise au microfilmage. Nous avons tout fait pour assurer une qualité supérieure de reproduction.

S'il manque des pages, veuillez communiquer avec l'université qui a conféré le grade.

La qualité d'impression de certaines pages peut laisser à désirer, surtout si les pages originales ont été dactylographiées à l'aide d'un ruban usé ou si l'université nous a fait parvenir une photocopie de qualité inférieure.

La reproduction, même partielle, de cette microforme est soumise à la Loi canadienne sur le droit d'auteur, SRC 1970, c. C-30, et ses amendements subséquents.

NL-339 (r. 88/04) c

Canada

National Library of Canada
Bibliothèque nationale du Canada

Canadian Theses Service
Service des thèses canadiennes

Ottawa, Canada
K1A 0N4

The author has granted an irrevocable non-exclusive licence allowing the National Library of Canada to reproduce, loan, distribute or sell copies of his/her thesis by any means and in any form or format, making this thesis available to interested persons.

L'auteur a accordé une licence irrévocable et non exclusive permettant à la Bibliothèque nationale du Canada de reproduire, prêter, distribuer ou vendre des copies de sa thèse de quelque manière et sous quelque forme que ce soit pour mettre des exemplaires de cette thèse à la disposition des personnes intéressées.

The author retains ownership of the copyright in his/her thesis. Neither the thesis nor substantial extracts from it may be printed or otherwise reproduced without his/her permission.

L'auteur conserve la propriété du droit d'auteur qui protège sa thèse. Ni la thèse ni des extraits substantiels de celle-ci ne doivent être imprimés ou autrement reproduits sans son autorisation.

ISBN 0-315-55583-1

Canada

THE UNIVERSITY OF ALBERTA

DESIGN STUDY OF A PIEZOELECTRIC COCHLEAR IMPLANT

BY

DAVID EUGENE KUSHNIR

A THESIS

SUBMITTED TO THE FACULTY OF GRADUATE STUDIES AND RESEARCH IN PARTIAL FULFILMENT OF THE REQUIREMENTS FOR THE DEGREE OF MASTER OF SCIENCE

DEPARTMENT OF ELECTRICAL ENGINEERING

EDMONTON, ALBERTA

FALL 1989

THE UNIVERSITY OF ALBERTA

RELEASE FORM

NAME OF AUTHOR: David Eugene Kushnir

TITLE OF THESIS: Design Study of a Piezoelectric Cochlear Implant

DEGREE: MASTER OF SCIENCE IN ELECTRICAL ENGINEERING

YEAR THIS DEGREE GRANTED: 1989

Permission is hereby granted to THE UNIVERSITY OF ALBERTA LIBRARY to reproduce single copies of this thesis and to lend or sell such copies for private, scholarly or scientific research purposes only.

The author reserves other publication rights, and neither the thesis nor extensive extracts from it may be printed or otherwise reproduced without the author's written permission.

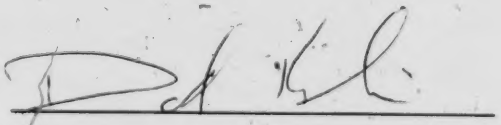

David Kushnir
#2005-8620 Jasper Avenue
Edmonton, Alberta
T5H 3S6

Date: October 13, 1989

THE UNIVERSITY OF ALBERTA

FACULTY OF GRADUATE STUDIES AND RESEARCH

The undersigned certify that they have read, and recommend to the Faculty of Graduate Studies and Research for acceptance, a thesis entitled "Design Study of a Piezoelectric Cochlear Implant" submitted by David Eugene Kushnir in partial fulfilment of the requirements for the degree of Master of Science in Electrical Engineering.

(Supervisor)

Date: 13-oct-1989

ABSTRACT

A design study of a multichannel piezoelectric cochlear implant is presented in this thesis. After reviewing the function of the inner ear and presenting the concept of piezoelectricity two possible implant designs are discussed. The results of experiments performed to measure pertinant electrical properties of the piezoelectric material considered for the implant and measure the potential field surrounding the implant are presented. These results are used in the design equations to determine the output of the implant inside the ear. Alternate materials and methods for achieving stimulation are also presented. Several mechanical and physiological considerations are presented as topics for further study.

TABLE OF CONTENTS

1. INTRODUCTION 1

2. ANATOMY 5

2.1 Outer and Middle Ear 5
2.2 Inner Ear 5
2.2.1 The Labyrinth 5
2.2.2 The Cochlea 6

3. AUDITORY MECHANICS 10

3.1 Mechanics of the Outer and Middle Ear 10
3.2 Mechanics of the Cochlea 11

4.PIEZOELECTRICITY 16

4.1 Piezoelectricity 16
4.2 Polyvinylidene Fluoride 16
4.3 Mechano-Electrical Properties 18

5. PROSTHESIS DESIGN 22

5.1 Conceptual Design 22
5.2 Theoretical Design Calculations 23

6. MATERIAL TEST 31

6.1 Voltage Constant Test 31
6.2 Internal Electrical Impedance Test 41
6.3 Voltage Field Pattern Measurements 47

7. DESIGN REVISIONS 57

7.1 Electrical Output 57
7.2 Other Considerations 61

8. ALTERNATE MATERIALS AND METHODS 65

8.1 Electrets 65
8.2 Alternate Methods 69

9. CONCLUSIONS 71

REFERENCES 74

APPENDIX I 79

LIST OF TABLES

6-1 : Voltage Constant Test Measurements 41

6-2 : Mean and Standard Deviation of Potential Field Accuracy Measurements 54

LIST OF FIGURES

2-1 :	Cross Section of the Cochlea	7
2-2 :	Cross Section of the Organ of Corti	8
3-1 :	The Uncoiled Cochlea	12
4-1 :	Coordinate System for Piezoelectric Film Properties	19
5-1 :	Cross Section of the Conceptual Implant in the Cochlea	23
5-2 :	Implant #1	24
5-3 :	Implant #2	24
6-1 :	Voltage Constant Test Apparatus	32
6-2 :	Solar Cell Assembly	33
6-3 :	Test Sample	34
6-4 :	Voltage Constant Test Measurement Circuit	36
6-5 :	Displacement of Cardboard Plate *vs.* Voltage Output of Solar Cell Assembly	38
6-6 :	Internal Impedance Test Apparatus	43
6-7 :	Internal Impedance Measurement Circuit	44
6-8 :	Test Sample With Load	46
6-9 :	Electrical Impedance of Test Samples *vs.* Frequency	48
6-10 :	Implant Model	50
6-11 :	Potential Field Measurement Apparatus	51
6-12 :	Plane of Field Pattern Measurement	53
6-13 :	Potential Field Around the Implant Model	55
8-1 :	Electret Transducer	66
A-1 :	A Square Membrane With Sides of Length 2a	80

INTRODUCTION

For hundreds of years man has tried to develop prostheses to replace missing limbs. The wooden leg is a typical example as is a hook used to replace a lost hand. Man has also tried to correct deficiencies of the senses. The most common example of this is eye glasses. Another example is the horns used around the turn of the century to aid the hearing of the elderly.

As time progressed these devices became more sophisticated and were better able to reproduce the functions they were designed to duplicate or assist. With the development of the transistor and the ensuing technological boom, prosthesis research has taken great leaps and bounds forward. In auditory prosthesis research, techniques in micro-fabrication and integrated circuit technology have led to the development of devices which can improve the hearing of hearing impaired individuals or restore some perception of speech in those people who are functionally deaf. It is these advances in auditory prosthesis research coupled with advances in material science which are the topics of this thesis.

Hearing aids are able to correct hearing disorders of many patients. For individuals who suffer from biological dysfunctions such as stereocilia damage, a number of implantable prosthetic devices have been developed over the last 25 years [2]. These devices are

designed to electrically stimulate the auditory nerve in order to restore some perception of sound. They all consist of a microphone to pick up incoming sound, a speech processor-transmitter to pass coded signals through the skin, an implanted receiver-driver to pick up these coded signals and a single or multi-channel electrode array implanted in the cochlea. Both single and multi-channel systems allow their users to distinguish between a wide variety of different sounds found in their daily lives. The single channel implants provide a limited perception of speech [1]. The multi-channel devices allow stimulation of discrete nerve populations and therefore show more promise for the perception of speech [2].

No current implant design, however, provides total speech perception and users must still rely heavily on lip reading to understand anything spoken to them. In order to have adequate speech recognition, stimulation of the ear must be provided over a continuous frequency range. In addition it would be desirable to make use of some of the ear's remaining abilities to eliminate as many external components as possible in order to simplify the design and usage of the device.

In this thesis a study is presented of a piezoelectric cochlear prosthesis which may provide a more continuous range of stimulation than is currently available, thereby providing a better perception of

speech for users of the implant. In addition, the prosthesis offers simplicity of design and does not require an external power source.

In chapter 2 some aspects of the anatomy of the ear are reviewed. Particular attention is given to the inner ear where the implant would be placed. It is here that the implant will convert sound energy into electrical energy.

In chapter 3 cochlear mechanics is discussed. It is necessary to have a thorough understanding of how the ear converts sound energy into electrical impulses in order that a device can be designed to duplicate the process.

The concept of piezoelectricity is discussed in chapter 4. What piezoelectricity is and how it can be used to stimulate the ear will be dealt with.

The process of designing the implant begins in chapter 5. Two designs are considered and the theoretical calculations for each are given.

In chapter 6 two experiments are described in which pertinent material properties of the piezoelectric film are tested. A third experiment is described in which the potential field patterns around a simulated implant are mapped.

In chapter 7 the theoretical calculations of chapter 5 are repeated using the information obtained in chapter 6. The load presented by the tissues of the ear is determined and this load is used to calculate the output

of each implant configuration to see if it can produce currents large enough to cause stimulation of the cochlear nerve. Additional concerns for the design of the implant are also discussed.

Alternate transducers and methods of stimulation are discussed in chapter 8. During the course of this research, several alternative methods were considered and some preliminary design work was performed.

Chapter 9 contains concluding remarks and lists some areas that merit further study.

2. ANATOMY

2.1 Outer and Middle Ear

The term "ear" refers to the entire conductive and sensorineural auditory system. It is divided into three sections: the outer ear, the middle ear, and the inner ear. The outer ear starts at the pinna, (the visible structure on the side of the head), leads down the ear canal and terminates at the *tympanic membrane* or *eardrum*. Beyond the tympanic membrane is the middle ear. It contains the *malleus*, *incus* and *stapes*; three small bones known collectively and the *ossicular chain*. The malleus connects to the eardrum and the footplate of the stapes attaches to the oval window of the inner ear. The ossicular chain acts as an impedance matching network which couples the vibrations of the eardrum to the fluid filled inner ear. At high sound intensities muscles attached to these bones inhibit their movement. Therefore the ossicular chain also acts as a gain control network to protect the inner ear from harmful sound intensities.

2.2 Inner Ear

2.2.1 The Labyrinth

The final part of the auditory system is the inner ear or *labyrinth*. It is a series of interconnected canals in the temporal bone of the skull. The labyrinth is actually made up of two structures, one inside the other. The outer structure is the bony labyrinth. It is the

actual hollowed out portion of the temporal bone. The inner structure is the membranous labyrinth. It is a series of interconnected sacs which generally conform to the the shape of the outer, bony labyrinth [3]. Both structures are full of fluid. The bony labyrinth contains a fluid called *perilymph*, which is analogous to cerebrospinal fluid [36], while the membranous labyrinth is filled with a fluid called *endolymph*.

The labyrinth structure can be further divided into three sections. The first contains the vestibular system responsible for balance and equilibrium. The second contains the auditory system, which is of primary concern here, and will be described in greater detail. The third and final section is called the *vestibule*, and it serves to interconnect the other two sections.

2.2.2 The Cochlea

The auditory portion of the labyrinth is called the *cochlea*. It is a hollow canal (typically 35 mm in length and 1 mm in width, narrowing slightly from base to apex) that spirals $2\frac{3}{4}$ turns around a central core of bone called the *modiolus*. A thin shelf of bone, known as the *bony spiral lamina*, extends into the canal from the modiolus for almost the entire length of the cochlea, stopping just short of the apex. The cochlea is divided in half by the *basilar membrane*, a tough yet highly flexible membrane which extends from the spiral lamina to the outer wall of the canal where it is held in place by the *spiral*

ligament. A second, thinner, membrane, *Reissner's membrane*, further divides the cochlea. It stretches diagonally from the bony spiral lamina to the outer wall of the canal where it too, is attached to the spiral ligament. Reissner's membrane also extends almost the entire length of the cochlea and attaches to the basilar membrane just short of the apex. The result is that the cochlea is divided longitudinally into three separate channels. The upper channel, formed by the outer wall and Reissner's membrane is called the *scala vestibuli*. The lower channel, formed by the basilar membrane and the outer wall, is called the *scala tympani*. The third

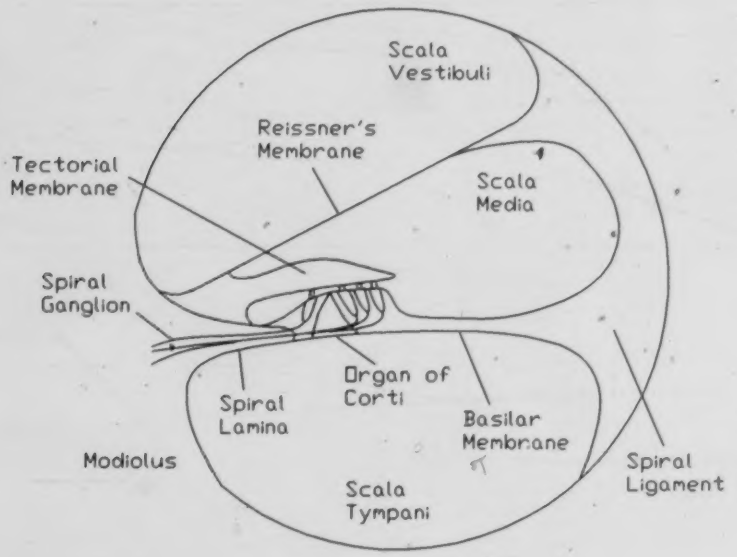

Figure 2-1: Cross Section of the Cochlea

channel is that formed by the basilar and Reissner's membranes; known as the *scala media* or *cochlear duct*. Figure 2-1 shows a cross section of the cochlear channel detailing the various structures inside. The scala tympani and scala vestibuli are part of the bony labyrinth portion of the labyrinth system and are filled with perilymph. Since the basilar and Reissner's membranes meet a short distance from the apex of the cochlea, a connecting channel called the *helicotrema* is formed allowing perilymph to communicate between the scales tympani and vestibuli. Both the scala tympani and scala vestibuli terminate at the bottom or *basal* end of the cochlea. The scala vestibuli terminates at the *oval window*, which is closed by the footplate of the stapes [3]. The *round*

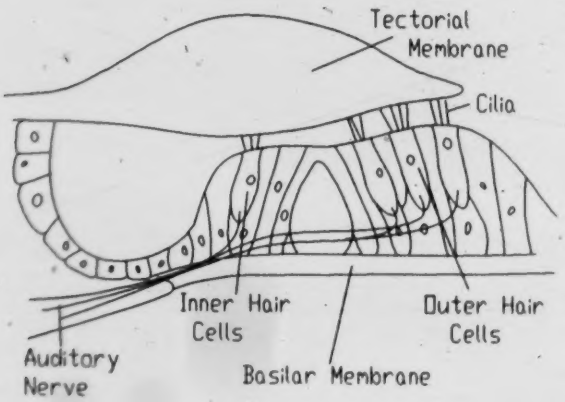

Figure 2-2: Cross Section of the Organ of Corti

window, a membrane covered opening located below the oval window in the vestibule, terminates the scala tympani. The scala media is a structure separate from the scalas tympani and vestibuli. It is part of the membranous labyrinth and is therefore filled with endolymph. It is the scala media that contains the actual hearing organ called the *organ of corti;* detailed in figure 2-2. The organ of corti is a complex structure which sits on top of the basilar membrane and extends for its entire length. It consists of four rows of hair cells called *inner* and *outer hair cells*, (1 inner and 3 outer rows), separated by various supporting cells. Each hair cell is innervated by one or more afferent and/or efferent nerve fibers. These nerve fibers pass from the hair cells through the bony spiral lamina and gather inside the modiolus where they form the cochlear branch of the *VIII cranial* or *auditory nerve*. At the top of each hair cell are small hair-like projections called cilia. The tops of the cilia are embedded in a gelatinous structure called the *tectorial membrane*. The tectorial membrane is in turn attached to the upper lip of the bony spiral lamina. The combination of basilar membrane, hair cells, cilia and tectorial membrane is responsible for converting vibratory stimulus into an electrical stimulus which the brain perceives as sound. How this conversion is achieved is described in the next chapter.

3. AUDITORY MECHANICS

3.1 Mechanics of the Outer and Middle Ear

We will begin this description of the hearing process at the outer ear where sound waves impinge on the eardrum causing it to vibrate. The intensity of the incident sound pressure is used as a reference in many studies of the cochlea (and in audiology) and it will be used as a reference in this thesis as well. Sound pressure is measured in units of "dB SPL" (Sound Pressure Level) and is calculated as follows:

$$P = 20\log\left(\frac{\text{Incident Pressure}}{\text{Threshold of Hearing}}\right) \text{ dB SPL} \qquad (2\text{-}1)$$

The hearing threshold in humans is typically as low as 20μPa (0 dB SPL) and incident pressures as high as 2000Pa can be tolerated without pain [5]. This gives the human ear a dynamic range of 140 dB SPL (calculated using Eqn. 2.1).

When the tympanic membrane vibrates in response to an auditory stimulus the three bones of the ossicular chain transmit these vibrations to the oval window of the inner ear. This causes the footplate of the stapes to vibrate in a reciprocating fashion, (much like the piston in an engine), causing the displacement of perilymph in the scala vestibuli.

As mentioned in Chapter 2, the ossicular chain acts

as an impedance transformer between the outer and inner ears. The cross sectional area of the oval window is approximately 19 times smaller than the eardrum. In addition the ossicular chain behaves like a lever with a lever ratio of approximately 1.3 [5]. These two facts combine to produce a pressure increase of 25 times as the sound is transmitted from outer to inner ear.

3.2 Mechanics of the Cochlea

At this point matters will be simplified by treating the cochlea as if it were straight instead of coiled and by assuming that the scala media acts dynamically as part of the basilar membrane [6]. This last assumption is supported by experiments performed by von Békésy [22], which show that Reissner's membrane vibrates in phase with the basilar membrane.

As the stapes travels inward, fluid is displaced in the scala vestibuli. Since perilymph is relatively incompressible, the pressure in the scala vestibuli increases and a pressure gradient results across the scala media. This difference in pressure causes the basilar membrane to deflect downward displacing fluid in the scala tympani, which in turn causes the round window to travel outward. As the stapes moves outward these movements reverse direction. This is illustrated in Figure 3-1. Figure 3-1a is a representation of an uncoiled cochlea. The dotted lines indicate the response of the various structures to the inward motion of the

stapes. The arrows indicate the direction of fluid flow. Figure 3-1b is a cross section of the point marked "x" in Fig. 3-1a. It can be seen how a pressure increase in the scala vestibuli causes Reissner's membrane and the basilar membrane to deflect in unison.

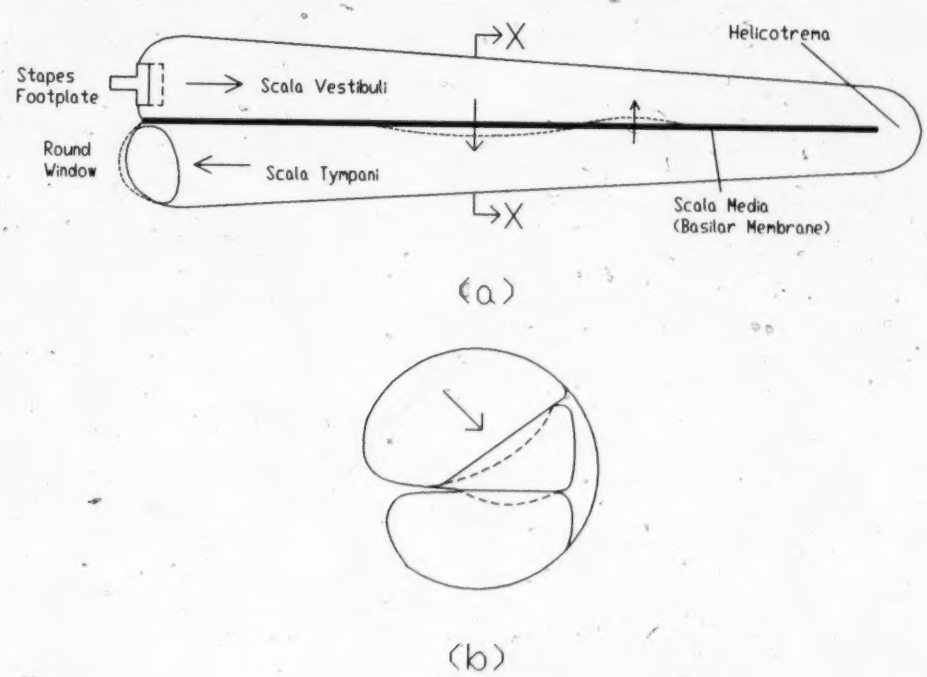

Figure 3-1: The Uncoiled Cochlea

The reciprocating motion of the stapes causes pressure "waves" to travel along the basilar membrane from base to apex, resulting in a travelling wave. This travelling wave is observed to increase in amplitude as it moves down the cochlea, until it reaches a maximum at a certain distance from the oval window after which the

amplitude diminishes rapidly. This is due to the mechanical properties of the basilar membrane.

As mentioned in the previous chapter the basilar membrane extends almost the entire length of the cochlea. It increases in width from about 0.1mm at the base to about 0.5mm at the apical end. The membrane also becomes less stiff as it travels from base to apex. This results in the basal end of the cochlea being more sensitive to higher frequency vibrations and the apical end being more sensitive to lower frequency vibrations. The basilar membrane acts therefore, as a type of spatial frequency filter where each input frequency resonates at a specific place on the membrane. It should be noted, however, that researchers do not believe that this is the only way in which the ear distinguishes sound [2,37-40].

As the basilar membrane vibrates up and down the organ of corti, sitting on top of it, moves up and down also. The tectorial membrane also moves in concert with the basilar membrane but not to the same degree. The basilar membrane (and the organ of corti) has a different pivot point than the tectorial membrane. The basilar membrane pivots at the tip of the bony spiral lamina while the tectorial membrane pivots at a point closer to the outer wall of the cochlea. This results in a relative motion between the two when the ear is stimulated. Recall from chapter two that the tops of the cilia of the hair cell in the organ of corti are embedded

in the tectorial membrane. When the ear is stimulated the relative motion between the tectorial membrane and the organ of corti creates a shearing action on the cilia. Some researchers believe this shearing action causes the hair cells to depolarize thereby triggering the nerve cells connected to them [13]. Others believe that the hair cells have a spontaneous discharge rate that is varied as the cilia bend [5]. Regardless of the method, the result is a train of action potentials each time the ear is excited.

For individuals who suffer from stereocilia damage the hair cells are destroyed or not functioning properly while at least part of the afferent nerves are intact. With the cochlear implant proposed in this paper it is expected that the function of the hair cells can be bypassed and that the auditory nerves can be stimulated by signals from the implant. This approach is similar to that taken in the design of existing multi-electrode cochlear implants described in chapter one. Both designs (ours and theirs) are based on the spatial frequency filtering abilities of the inner ear mentioned earlier. Since research has so far failed to determine exactly how the ear responds to complex signals it is believed that this frequency filtering approximation will suffice for a first generation design of this type. There is, however, one significant difference between our proposed design and the implants that already exist. We seek to use the

superior filtering capabilities of the middle and inner ear itself rather than a man made approximation contained in an external processing unit. This may produce a better perception of speech than is available with current designs.

Before we can consider the design procedure for the implant, one more topic must be introduced: piezoelectricity. In the next chapter the phenomenon of piezoelectricity and how it will be used in the implant design will be discussed. The particular piezoelectric material chosen for the implant, its properties, and the reason for its selection are also discussed.

4. PIEZOELECTRICITY

4.1 Piezoelectricity

Piezoelectricity literally means pressure electricity. It is the term used to describe the phenomenon discovered by French physicists Jacque and Pierre Curie. They discovered that a quartz crystal would deform when a voltage was applied to it. In addition, when that same crystal was mechanically deformed a voltage would be generated across the faces of the crystal.

Quartz is not the only naturally occurring piezoelectric material. Rochelle salts, tourmaline as well as human and animal bone and tendon also exhibit piezoelectric properties. In his continuing efforts to improve on nature, man has been able to synthesize many piezoelectric materials. One of the most promising, for our purposes, is PolyVinyliDene Fluoride or PVDF, essentially a specially processed sheet of plastic. This is the material we have chosen to test for use in the cochlear prosthesis.

4.2 Polyvinylidene Fluoride

Polyvinylidene fluoride is a semi-crystalline high molecular weight polymer. It is formed by fluorine, carbon and hydrogen atoms chained in repeating CH_2 - CF_2 units. PVDF has many uses in its unpolarized natural state. In the chemical industry extensive use of PVDF is

made for the construction of pipes, valves etc. due to its excellent resistance to corrosive substances (this property makes it suitable for use in a body fluid environment). It is also used in a variety of products from automobile warning stickers and pin-striping to the base for certain metal finishes.

A carefully controlled process is followed to give the film its piezoelectric properties. First the two faces of the film are metallized using vacuum deposition. This provides intimate electrical contact during polarization as well as in subsequent use. Next the film is stretched at an elevated temperature to align the polymer chains in the stretch or machine direction. The film is then placed in an intense electric field (the poling field) to polarize it. This causes the electric dipoles formed by the fluorine and hydrogen atoms to align through the thickness of the film (normal the the surface). Finally the film is allowed to cool in the poling field to lock in the piezoelectric properties. This produces a piezoelectric material with anisotopic or directionally dependent properties. That is, its mechanical, electrical and electromechanical properties differ in different directions. Figure 4.1 shows the coordinate system that will be used when describing these directionally dependent properties. In order to fully understand the various properties of PVDF film it is necessary to use tensors to relate vectors of

polarization or electric field to tensors of mechanical stress or strain. This would involve more detail than needs to be presented here. Fortunately, we can limit ourselves to one key equation presented in the next section of this chapter.

The PVDF samples considered for the cochlear prosthesis were obtained from the Pennwalt Corporation under the brand name of KYNAR Piezo Film. A technical manual was included along with the PVDF samples. It provided a complete theoretical and numerical description of the properties of KYNAR piezoelectric film and included suggestions on applications and handling. Specifications, material constants and properties discussed in the following sections or chapters of this paper were obtained from this manual. The reader is referred to this manual as well as the other references listed in the bibliography for a more thorough understanding of the theory and properties that govern piezoelectricity.

4.3 Mechano - Electrical Properties

Polyvinylidene fluoride's ability to convert mechanical energy into electrical energy is the property of the film that interests us the most. When PVDF is subjected to an evenly distributed compressive (negative) or tensile (positive) stress in the 1, 2 or 3 directions (see Fig. 4-1), a voltage is generated across the upper and lower (3 direction in Fig. 4-1)metallized surfaces of

the film. This voltage is governed by the following equation:

$$V_o = g_{31} X_1 t \qquad (4\text{-}1)$$

Where: V_o = the voltage which appears across the electrodes on the upper and lower faces.

g_{31} = the piezoelectric voltage constant for KYNAR piezoelectric film.

i = the direction of the applied stress. ie. i=3 for a compressive stress in the 3 direction (normal to the surface of the film).

X_1 = the magnitude and direction (positive or negative) of the applied stress.

t = the thickness of the film.

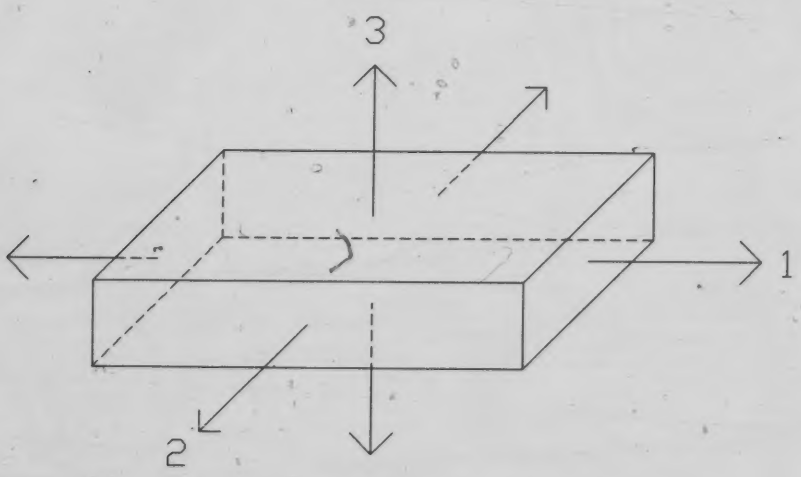

Figure 4-1: Coordinate System for Piezoelectric Film Properties

For example consider a 1cm x 1cm by 28μm thick sample of piezoelectric film subjected to a compressive stress of

100kPa normal to the surface of the film (the 3 direction):

$g_{33} = -339 \times 10^{-3} \frac{Vm}{N}$ (from technical manual)

$X_3 = -100{,}000$ Pa (compressive)

$t = 28\ \mu m$

$V_o = g_{33} X_3 t$

$V_o = (-339 \times 10^{-3})(-100{,}000)(28 \times 10^{-6})$

$V_o = 0.949$ V

The values of the piezoelectric voltage constants are dependent not only on the process involved in developing the piezoelectric effect but also on the mechanical boundary conditions imposed on the film during excitation. If, in the above example, the 100kPa force immobilized the film preventing movement in the 1 and 2 directions then the value of g_{33} would drop to $-207 \times 10^{-3} \frac{Vm}{N}$, a reduction of almost 40 percent!

The high degree of piezoelectricity exhibited by PVDF is not its only appealing feature. Its high resistance to corrosive substances makes it attractive for use in the corrosive saline environment inside the body. It has been used as a transducer through a range of frequencies from DC to the GHz range and provides a flat mechanical frequency response [12]. The elevated temperatures inside the body (37 °C) will actually serve to increase the piezoelectric activity slightly. PVDF is

10 times more compliant than ceramic piezoelectrics yet it is mechanically tough [12]. It also has a good acoustic impedance match to water. KYNAR film is available in standard thicknesses of 6μm, 9μm, 16μm, 28μm (the size of our samples), 52μm and 110μm and custom thicknesses can be produced by laminating different sizes together, thereby allowing us to choose a thickness to yield optimum results.

5. PROSTHESIS DESIGN

5.1 Conceptual Design

In the last three chapters we have described the various parts of the ear and how they function and some aspects of piezoelectricity were introduced. We will use that information as the basis for a design study of a cochlear implant.

Suppose a piece of PVDF film were placed against the basilar membrane in the scala tympani. It would be held in place by some sort of frame and would span the basilar membrane while extending from the round window to as far as is is possible for the device to be inserted. One face of the film would rest against the basilar membrane and the bony spiral lamina and the other would be exposed to the perilymph of the scala tympani. A cross sectional view is provided in Figure 5-1. Recall from chapter 3 that as sound enters the ear, the stapes creates pressure waves in the scala vestibuli. This in turn causes the basilar membrane to deflect. As the basilar membrane moves up and down it exerts a varying pressure on the PVDF film, which responds by producing a varying voltage across its two faces. If large enough this voltage will produce ionic currents of sufficient magnitude in the fluids and tissues of the inner ear to depolarize nearby hair cells or nerve fibers, giving the subject a perception of sound. A prosthesis of this kind would

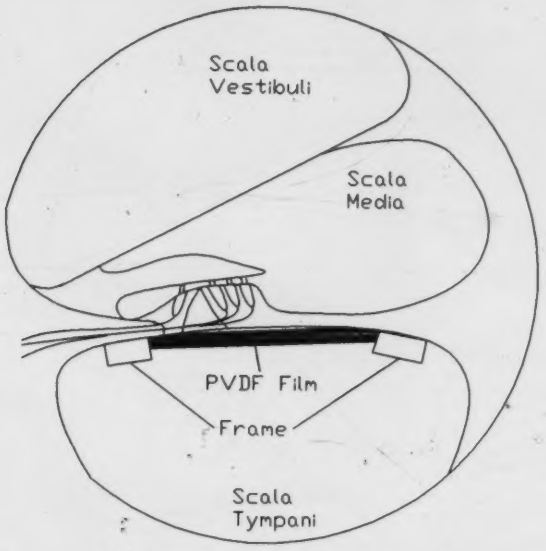

Figure 5-1: Cross-Sectional View of the Conceptual Implant in the Cochlea.

make use of the ear's remaining capabilities and thus simplify the design. In the next section the theoretical electrical calculation for the implant is presented. Several mechanical and physiological considerations are covered in a later chapter.

5.2 Theoretical Design Calculations

Two possible designs were considered for the implant. The first, hereafter referred to as implant #1, consists of a single piece of film 20 mm long and 1 mm wide held in a curved frame as illustrated in Figure 5-2. The film would be tapered slightly to aid insertion. When the assembly is placed inside the cochlea the frame will hold the film against the basilar membrane. The

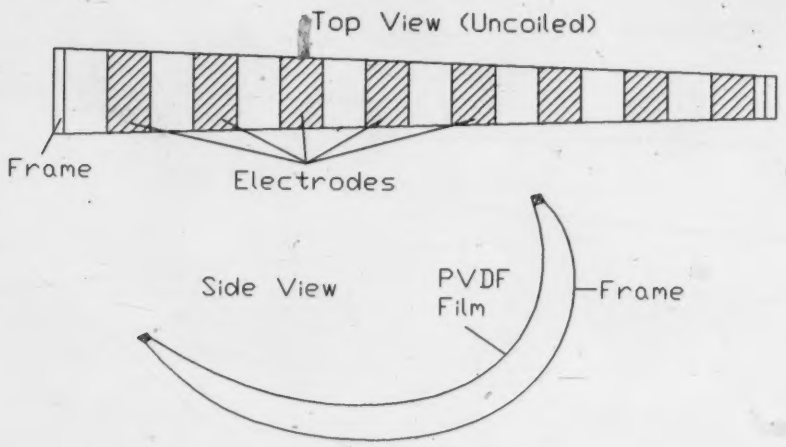

Figure 5-2: Implant #1.

outside face, (the face not touching the basilar membrane), would then be metallized to form a return

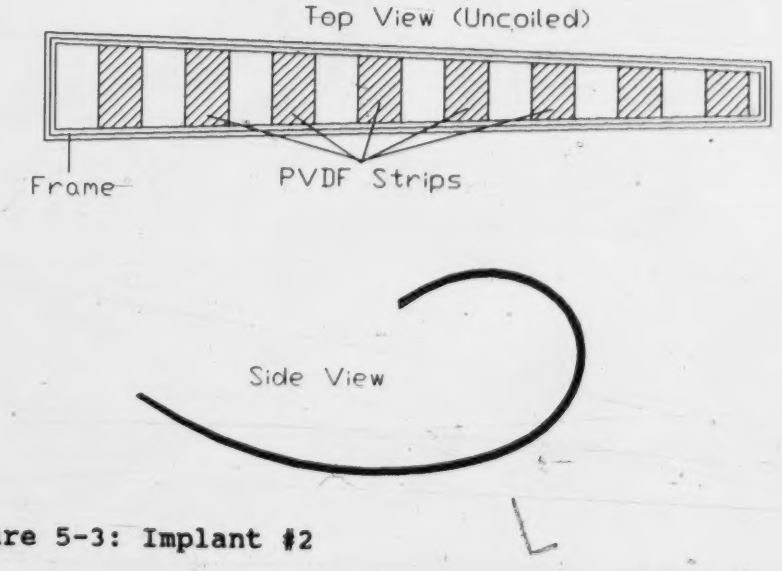

Figure 5-3: Implant #2

electrode. Another possibility would be to metallize both faces and create electrode sites by etching patterns into the metallization.

The second design, hereafter referred to as implant #2, consists of several pieces of film 1 mm wide, (one for each stimulation site), held in a curved frame as shown in Figure 5-3. The 1 axis of the film would be oriented perpendicular to the long axis of the implant. The radius of curvature of the frame would be smaller than that of the cochlea and the assembly would clamp itself against the basilar membrane. The design of the prosthesis is based on a number of assumptions and conclusions. These are unavoidable since pertinent measurements have never been performed on a living human cochlea. The only available data on the pressures in the cochlea and the movement of the basilar membrane has come from animal studies. Pressures in the scala vestibuli and scala tympani in response to auditory stimulus have only been measured in cats and guinea pigs [7,8]. Is is assumed these measurements are valid for the human cochlea as well. Because it is unknown exactly how the basilar membrane responds to complex sounds, stimulation of only a single tone (1000 Hz) will be considered. This will produce only one small stimulation site at a time. As a design example, a stimulation site 1 mm x 1 mm somewhere in the second turn of the cochlea is chosen.

When the basilar membrane deflects downwards (or

upwards) The pressure difference across the cochlear duct exerts a compressive force on each implant in the 3 direction. Implant #2 also experiences a second type of force; an internal tensile force. This results when the film is forced to deflect but its sides are not allowed to move; they are held in place by the frame.

As mentioned earlier the only available data on intracochlear pressures is from guinea pigs and cats. Dancer and Franke [7] have measured the pressures in all three turns of the guinea pig cochlea and it is their data which we are using. For stimulus levels of 100 dB at the tympanic membrane Dancer and Franke have measured pressures in the scala tympani of between 122 dB and 130 dB in the second turn of the cochlea. Nedzelnitsky's [8] measurements of the pressures in cat cochleas indicates that the response to stimulus is linear to 140 dB. We assume this is true for guinea pigs as well. This means that scala tympani pressures of 162 dB to 170 dB will occur for stimulus pressures of 140 dB. We will use an average value of 166 dB for our calculations.

Timoshenko and Woinowsky-Krieger [9] have done theoretical work with thin plates and shells and their results are used here to calculate the tensile forces in the film of implant #2. Since PVDF film is extremely thin and has little flexural rigidity each site was modeled as a thin square membrane. For a square membrane subjected to a 3990 Pa(166 dB SPL) pressure normal to and

distributed evenly over its surface, an internal membrane stress of 618.4 kPa is produced. The reader is referred to Appendix 1 for detailed calculations of this result. It should be noted that stimulation of the film by the basilar membrane will not produce an evenly distributed force. Only a few simple problems concerning the stresses inside a membrane have been published by the two authors above [9]. This example was chosen due to its similarity to our problem. These approximations should, however, give us results adequate enough to determine the feasibility of our design.

Since the film in implant #2 is clamped by the frame and is not allowed to move in the 1 direction this tensile stress acts like a positive stress in the 1 direction. We can now use Eqn. 4-1 to compute the voltage developed across the faces of the film. Since stress is in the 1 direction we must use the voltage constant g_{31}. The relevant properties given by the manufacturer are as follows:

$$g_{33} = -339 \times 10^{-3} \frac{Vm}{N}$$

$$g_{31} = 216 \times 10^{-3} \frac{Vm}{N}$$

$$t = 28\mu m$$

$$\varepsilon_o = 12$$

From Appendix I:

$$X_1 = 618.4 \text{ kPa}$$

Equation 4-1 yields:

$$V_1 = g_{31} X_1 t$$

$$= (216 \times 10^{-3})(618.4 \times 10^{3})(28 \times 10^{-3})$$

$$V_1 = 3.74 \text{ V}$$

We can also calculate the voltage produced on the film, for both implants, as a result of the pressure difference between the scala vestibuli and the scala tympani. This pressure difference exerts a compressive stress in the 3 direction. Eqn. 4-1 yields:

$$V_2 = g_{33} X_3 t$$

$$= (-339 \times 10^{-3})(-3990)(28 \times 10^{-6})$$

$$V_2 = 37.87 \text{ mV}$$

This will be the voltage output of implant #1. Summing V_1 and V_2 produces the output voltage of implant #2:

$$V_o = V_1 + V_2$$

$$= 3.74 + 0.04$$

$$V_o = 3.78 \text{ V}$$

The piezoelectric film is acting not unlike a power supply, supplying current to the auditory nerves. Therefore, it would be prudent to calculate the internal impedance of the film. This impedance will restrict the current output of the film and it is necessary to know to what degree. This means that when either implant is placed inside the ear its actual output will be less than the 'no load' voltages calculated above.

The film acts essentially like a parallel plate capacitor. It consists of two flat metal electrodes separated by a dielectric. We can therefore calculate its capacitance by using:

$$C = \frac{\varepsilon\varepsilon_o A}{d} \qquad (5\text{-}1)$$

Where: ε = The dielectric constant of PVDF.

ε_o = The dielectric constant of free space.

A = The area of the electrodes.

d = The spacing between the electrodes.

The dielectric constant of PVDF is 12. For a 1 mm x 1 mm by 28μm thick piece of film the capacitance is:

$$C = \frac{(12)(8.85 \times 10^{-12})(0.001 \times 0.001)}{0.000028}$$

$$C = 3.79 \text{ pF}$$

The impedance at 1000 Hz can now be determined:

$$Z = \frac{1}{2\pi fC} \qquad (5\text{-}2)$$

$$Z = \frac{1}{(2\pi)(1000)(3.79 \times 10^{-12})}$$

$$Z = 41.96 \text{ M}\Omega$$

We can therefore think of the PVDF film as a pressure actuated voltage source with a frequency dependent internal impedance connected to a load. This load represents the tissues and electrolytes of the inner ear. The perilymph of the scala tympani has a resistivity of 50-65 Ω-cm [10,11]. The resistivity of the bone and the surrounding tissue differs from this value by a factor of about 2 [11]. This moderately low resistivity indicates that the fluid and structures surrounding the implant will act as a large load on the film reducing its output. However, nerve stimulation depends on the density of the stimulation current flowing through it. Even if the output of the film is reduced nerve depolarization will

still occur if the current density flowing through the nerve membrane is large enough. The nerve will also depolarize if the implant produces a voltage gradient of sufficient magnitude along its length. In the following chapter an experiment to determine the voltage potential pattern that would be produced by our prototype implant is presented. In addition the voltage constant g_{33} and the internal impedance of the film are also tested. Small variations in the manufacturing process may cause the constants to vary in a favorable manner.

6. MATERIAL TESTS

6.1 Voltage Constant Test

When a manufacturer states a specific tolerance or rating for a product, this is often a minimum value which can be guaranteed in every product produced. Sometimes however, these products perform better than the manufacturers minimum ratings. It was desired to find out if this applied to the voltage constants of the PVDF film. Specifically, the value of g_{33} was tested in five different samples to see if any of them exhibited a higher voltage constant which would increase the output of the implant.

To determine the value of g_{33} an apparatus was used to apply a pressure of a known magnitude in the 3 direction (normal to the surface) to each sample. The resulting voltage was then amplified and its value used to calculate the voltage constant g_{33}. The test apparatus is shown in Figure 6-1. The loudspeaker acts as the forcing mechanism. It converts an alternating electrical signal into a reciprocating motion. The resulting alternating force is coupled to the sample through a pair of connecting rods, one of which is attached to the speaker cone. The other rod terminates in a piston which is used to exert force on the sample. Mounted between the two rods is a linear spring. The spring is used to determine the force which the speaker

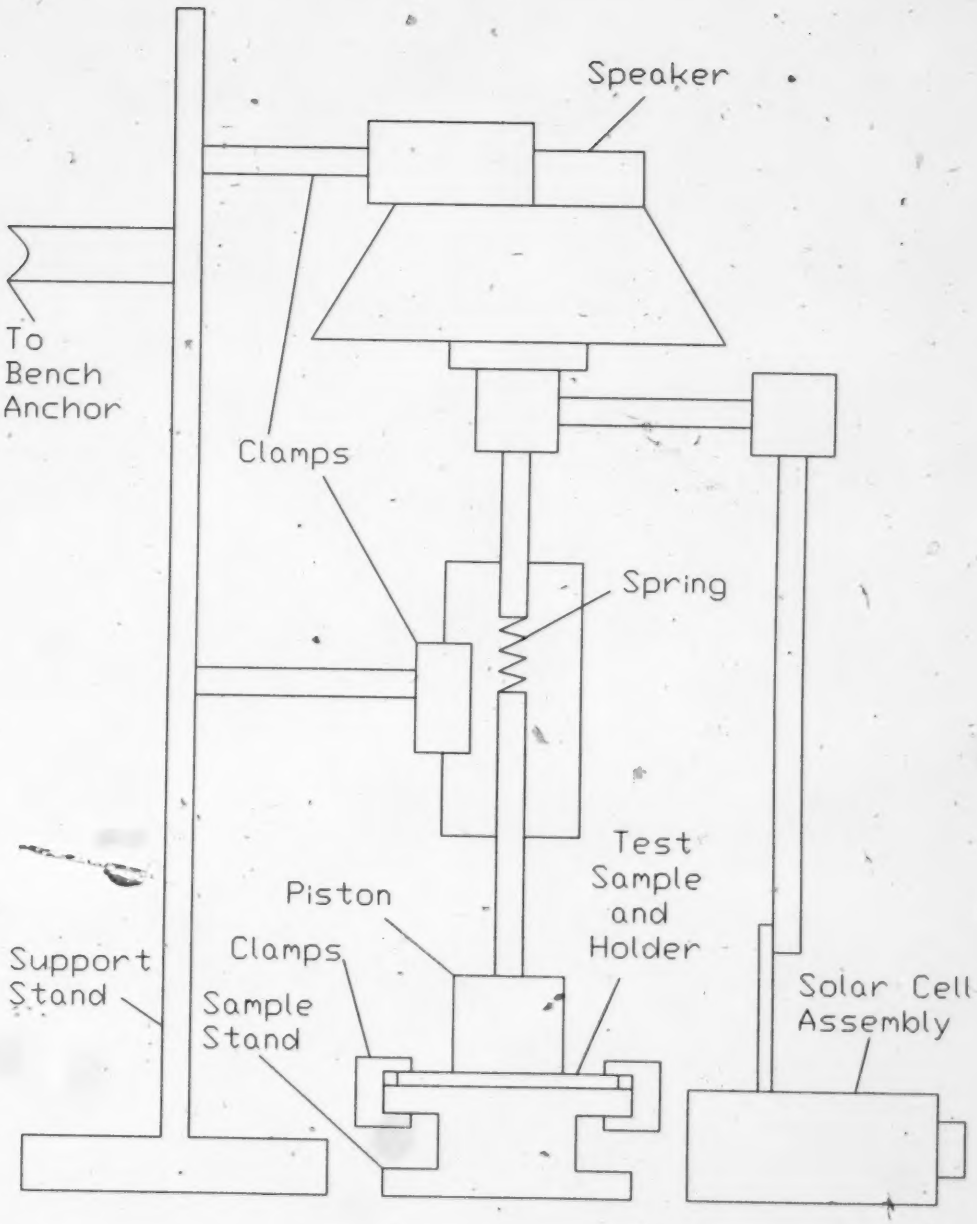

Figure 6-1: Voltage Constant Test Apparatus

exerts on the sample. Since the force on a spring is a linear function of the distance that the ends of the spring travel (F = kx), we need only to determine the distance which the upper connecting rod travels in order to calculate the force exerted on the test sample. This is accomplished by using the solar cell assembly shown in Figure 6-2. A cardboard plate passes between a solar cell and a light source. The change in the output of the

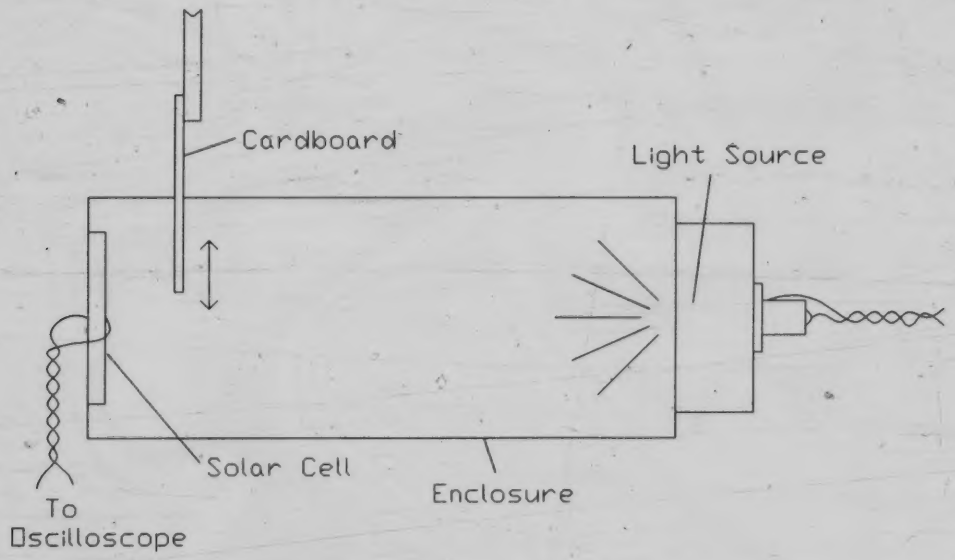

Figure 6-2: Solar Cell Assembly

solar cell is proportional to the displacement of the cardboard shield which is attached to the upper connecting rod.

The sample itself was placed in a special holder provided by the manufacturer. It is a piece of fiberglass board with a metal trace (to make electrical

contact with the bottom face of the test sample) and a clamp. The clamp is nothing more than a second smaller piece of fiberglass board with a metal trace on it. It can be attached to the main board to hold the test sample in place and provide electrical contact with the top face of the sample. This holder allows non-destructive and non-permanent contact to be made with both sides of the film simultaneously. The holder was slightly warped when it was received from the manufacturer. It was discovered that the holder would deflect when it was subjected to the force produced by the speaker. This deflection would introduce a substantial error into the data obtained from the spring. In addition, a warped holder would prevent the force from the speaker from being evenly distributed over the surface of the sample. To solve both of these problems the holder was flattened by clamping it to an aluminum base plate. The connecting rods in the

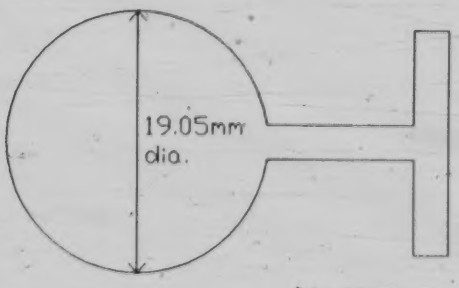

Figure 6-3: Test Sample

apparatus were also made out of aluminum to reduce their mass and help eliminate resonant vibrations.

Each film sample was cut to the shape shown in Figure 6-3. The circular area is the same diameter as the piston pressing on it. The thin rectangular section connected to the circle provides an electrical connection between the circle and the second rectangular area which is used to connect with the contacts of the sample holder. The sample is cut into the shape of the piston so that the applied force is distributed evenly over the entire sample. The manufacturer states that if the applied force is concentrated on a smaller area, the output voltage would not increase proportionally to the increase in force. For this reason we can neglect the effects of the two connecting pieces (their combined area is small compared to the area of the circle) on our measurement of g_{33}.

In order to measure the voltage output of the film a high impedance buffer - filter - amplifier circuit was used. The schematic diagram of this circuit is shown in Figure 6-4. U1 is an LF351 J-FET Op Amp wired as a voltage follower. R1 is used to supply the bias current needed by the op-amp since the test sample cannot. Unfortunately, the input impedance of the circuit is dropped from approximately $10^{12}\Omega$ to 144 MΩ, the value of R1. However, this should be of little consequence since R1 is 10 times the output impedance of the test sample

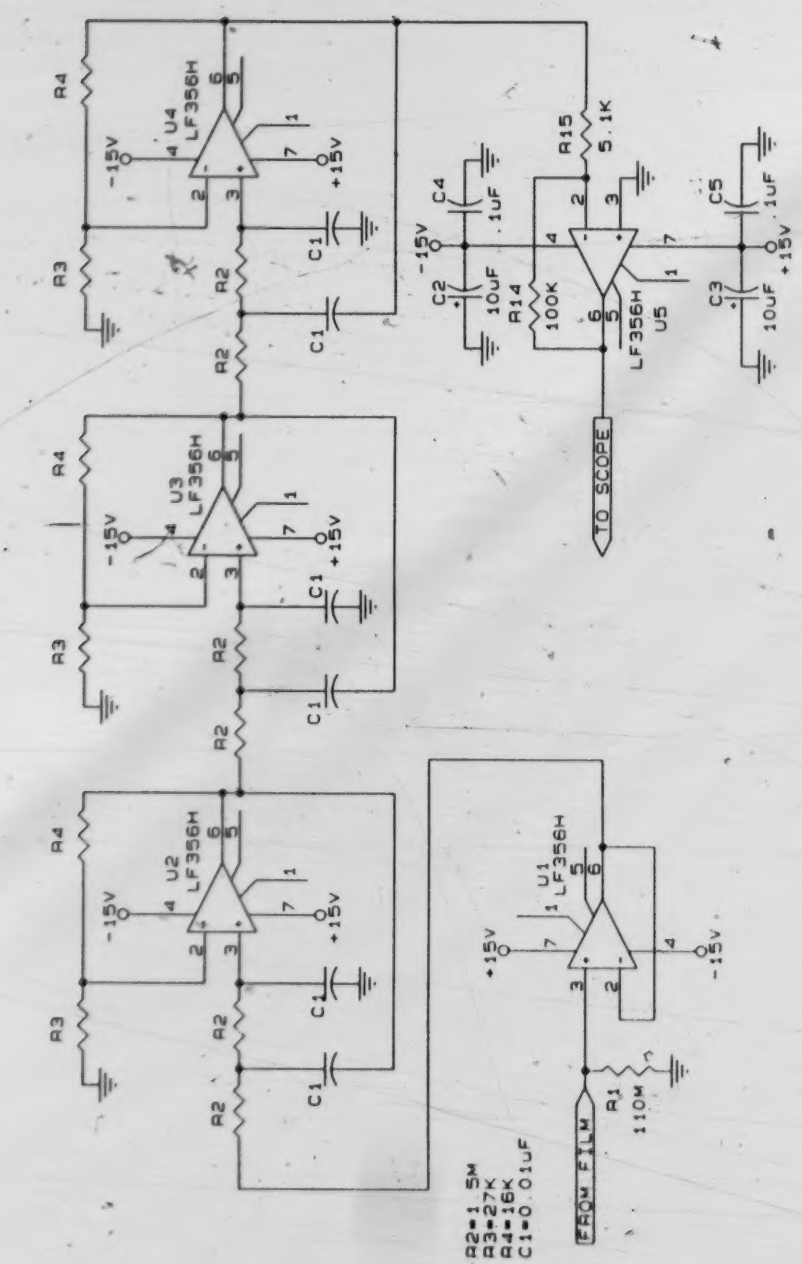

Figure 6-4: Voltage Constant Test Measurement Circuit

(approximately 14.7 MΩ @ 10 Hz calculated using the method used in chapter 5). U2, U3 and U4 are three second order Butterworth low pass filters each with a cut off frequency of 10 Hz. The sensitivity and broad band characteristics of PVDF film make it susceptible to a wide range of electromagnetic interference (especially 60 Hz) [12]. Accordingly, the low pass filter was used to eliminate the interference as well and any other spurious signals. Finally the signal was amplified by U5 to provide a suitable signal level for display on an oscilloscope. The overall gain of the circuit at the 10 Hz stimulation frequency was measured to be 33.

In order to determine the distance traveled by the speaker cone it was necessary to calibrate the solar cell assembly. As seen in Figure 6-2, a cardboard plate moves up and down in front of the solar cell varying the amount of light striking it. To determine the output vs. distance relationship, the plate was first attached to a micrometer. It was then inserted an arbitrary distance into the solar cell assembly. The insertion distance was increased in 0.25 ± 0.005 mm steps and the corresponding voltage output was measured. Figure 6-5 shows the distance vs. voltage plot using the data obtained by the calibration procedure. This graph allows us, using any arbitrary starting voltage, to determine the displacement of the speaker cone and thus the force exerted on the test sample.

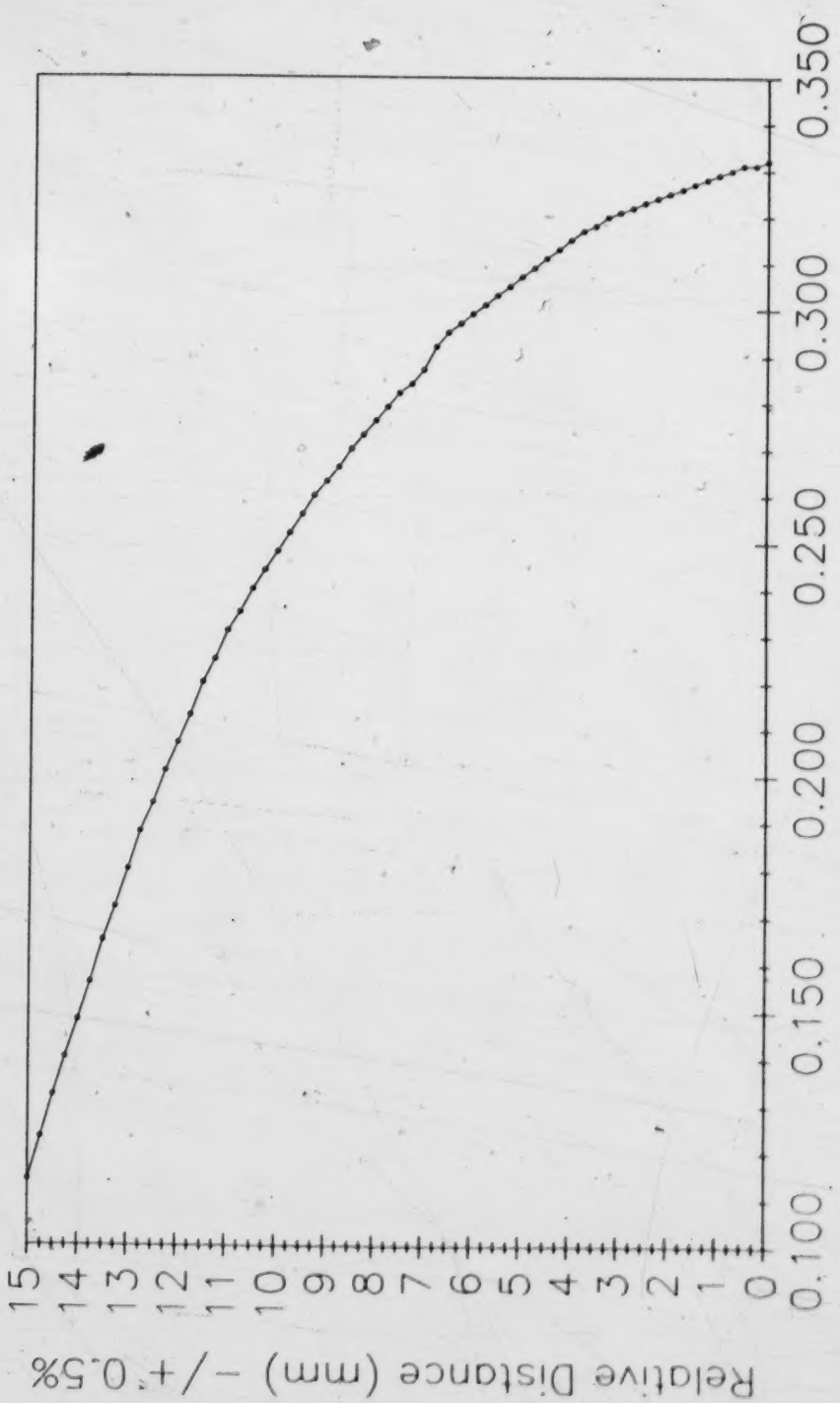

Figure 6-5: Displacement of Cardboard Plate *vs.* Voltage Output of the Solar Cell Assembly.

Five samples were tested to determine their g_{33} voltage constants. Each sample was placed in the film holder with its circular portion aligned under the piston. The speaker was lowered so that the upper connecting rod compressed the spring slightly. This provided an arbitrary bias force to ensure that the spring was always compressed even when the upper rod reached its point of maximum upward displacement. The speaker was then driven sinusoidaly at 10 Hz causing a sinusoidaly varying force to be impressed on the film. It was found that excessive movement of the speaker cone caused spurious vibrations in the support bracket which were in turn transmitted to the film. Therefore, the amplitude of the driving signal was chosen low enough to eliminate these vibrations. Since the available digital multimeters would not measure signals below 45 Hz, the output of both the solar cell and the film amplifier were displayed on a dual channel oscilloscope. The voltage error was no more than 25 mV. The following procedure was used to calculate g_{33} for each sample:

Test Bed Constants:

Amplifier gain @ 10 Hz = 33.00

Spring constant = 0.0584 ± 0.0001 N/mm

Area of piston = 0.285×10^{-3} m^2

<u>Sample #1</u>

Amplifier output = 80 mV ± 1.3%

$$\%\ \text{Film output} = \frac{0.080}{33.00}\ V = 2.42\ mV \pm 1.3\%$$

Solar cell base voltage = 247 mV
(Voltage of the cell when speaker is not moving)

Cell voltage variations = +6 mV, -7 mV ±25 mV
(Corresponding to speaker travel)

Figure 6-5 is now used to determine the amount of speaker cone travel. Using the solar cell base voltage as a starting point we find the points 6mV above and 7mV below the starting point. The difference in distance represents the distance traveled by the speaker cone in compressing the spring. According to Figure 6-5:

Speaker cone travel = d = 1.00 mm ± 6.4%
(peak to peak)

Force on the spring = F = kd = 0.0584 * 1.00

$$F = 0.058\ N \pm 6.5\%$$

Pressure on the film = X = -(F/area of piston)

$$X = -(0.058/0.285 \times 10^{-3})$$

$$X = -203.51\ Pa \pm 6.5\%$$

We now calculate g_{33} using equation 4-1:

$$V_o = g_{33} X_3 t$$

$$0.00242 = g_{33}(-203.51)(28 \times 10^{-6})$$

$$g_{33} = -0.42\ \frac{Vm}{N} \pm 7.8\%$$

The results of all five samples are tabulated in Table 6-1. The value of g_{33} specified by the manufacturer is also included for comparison. It can be seen that all five samples show a value of g_{33} greater than that given by the manufacturer. The mean value of all five samples is -1.03 Vm/N and the standard deviation

TABLE 6-1: Voltage Constant Test Results

Sample	g_{33} $(\frac{Vm}{N})$ ± 7.8%
1	-0.42
2	-1.40
3	-1.06
4	-1.48
5	-0.77
mfr. data	-0.339

is 0.39 Vm/N. The manufacturer's value is in the middle of the second standard deviation below the mean. This indicates that either the samples are of poor quality, (we can expect only about 90% to have values greater than -0.339 Vm/N), or that a small measurement error is present in the results. The fact remains, however, that all five samples have increased values of g_{33}. This will increase the output calculated in chapter 5. However due to the high internal impedance of the film even this increase in output may not provide adequate stimulation. Therefore a second test was performed to examine the electrical impedance of the five samples.

6.2 INTERNAL ELECTRICAL IMPEDANCE TEST

The high internal impedance of the PVDF film severely limits the current output of the film. In the preceding section it was shown that there are deviations in the value of the voltage constant g_{33}. It was decided to measure the internal impedance of the five samples at frequencies between 600Hz and 1000Hz to see if significant variations existed since these variations

would have a direct effect on the output of the film.

Figure 6-6 illustrates the test apparatus. As before a loudspeaker is used to apply a force to the film. The samples used in the previous experiment were used again for this test. Each sample was placed over a 2 mm diameter hole drilled in a support plate. A cover plate with a matching hole was placed on top of the film and used to hold the sample in place. This is illustrated in Figure 6-6b. Both the support plate and the cover plate had copper traces on them to allow electrical contact with both sides of the test sample. The support plate was attached to the speaker frame. When the speaker was driven, the reciprocating motion of the cone resulted in a varying air pressure inside the cone which in turn exerted a varying force upon the test sample. It was noted that covering the speaker completely with the sample support plate produced unwanted resonant effects and therefore the size of the plate was reduced to allow the air to pass freely around it.

The amplifier circuit required modification due to the change in stimulation frequencies. In order to remove 60 Hz interference from the test sample, three second order Butterworth high pass filters with a cut off frequencies of 600 Hz were substituted for the low pass filters in the circuit of the voltage constant test. To remove any high frequency noise amplified by the high

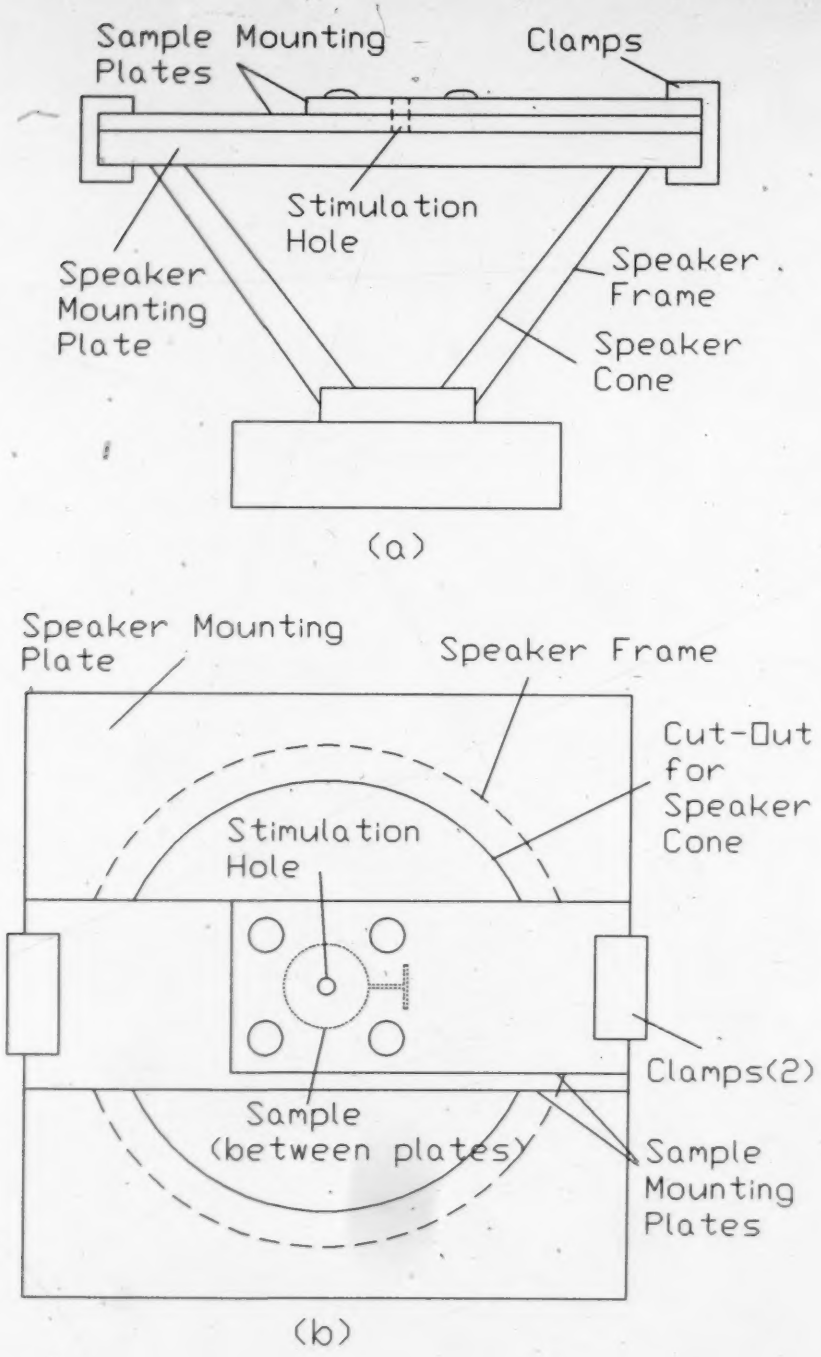

Figure 6-6: Internal Impedance Test Apparatus

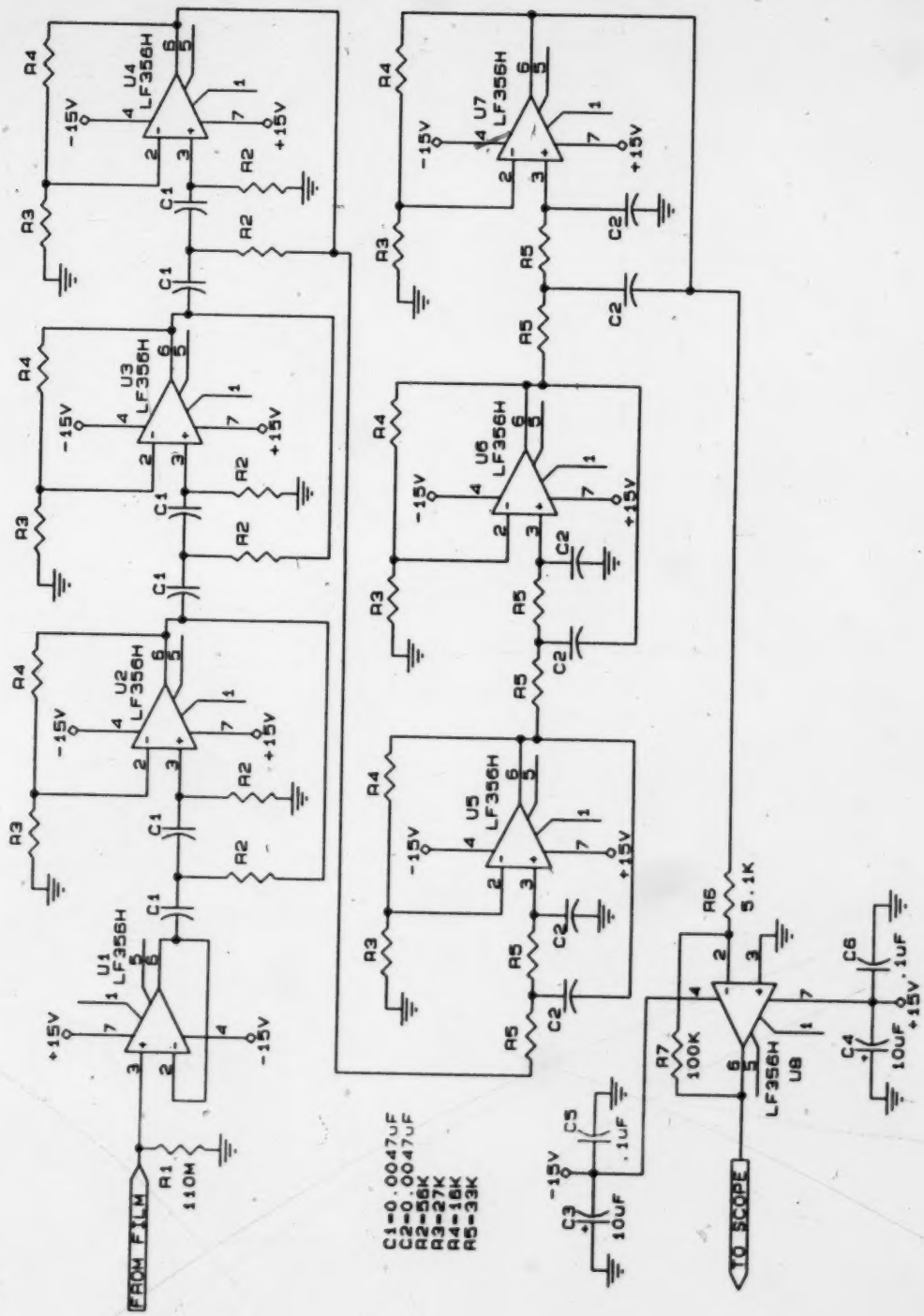

Figure 6-7: Internal Impedance Measurement Circuit

pass filters three second order Butterworth low pass filters with a cut off frequencies of 1000 Hz were added. These filters were used to completely reject all but the specified test frequencies. The complete circuit is given in Figure 6-7. As in the previous test a high impedance voltage follower was used as a buffer in front of the filter and an amplifier is used after it.

In order to measure the current output of the test sample and thus determine the internal impedance, a load resistor R_L was connected across the film. Resistor values of 100K and 56 K were used to collect output data. The film was stimulated at 600 Hz, 700 Hz, 800 Hz, 900 Hz and 1000 Hz to observe how the impedance varied with frequency. Each measurement was repeated five times and the average value of the impedance was calculated. For all tests the input voltage to the speaker driver was kept constant. Even though the frequency response of the speaker was not flat, thus causing the SPL to vary with frequency, the methods used to calculate the impedance negated any effects of changing input SPL. As long as the SPL remained constant for all measurements at a particular frequency, the impedance could be calculated. The following is a sample calculation to illustrate the method used to calculate the impedance of each sample:

The test sample and the load are illustrated in Figure 6-8. V_F is the voltage produced by the test sample. V_O is the voltage across the load R_L and I_L

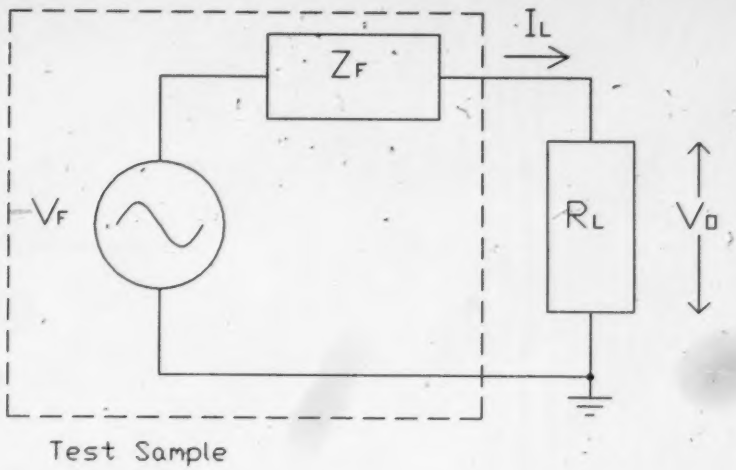

Figure 6-8: Test Sample With Load

is the current through it. R_F is the internal electrical impedance of the test sample. As an example we choose Sample #1 at 600 Hz:

$R_{L1} = 56k\Omega$ $V_{O1} = 19.8$ mV

$R_{L2} = 100k\Omega$ $V_{O2} = 32.4$ mV

$V_{F1} = I_{L1}R_F + V_{O1}$ where $I_{L1} = V_{O1}/R_{L1}$

$V_{F2} = I_{L2}R_F + V_{O2}$ where $I_{L2} = V_{O2}/R_{L2}$

Since the stimulation pressure was kept constant for both loads $V_{F1} = V_{F2}$. Therefore:

$$\frac{V_{O1}}{R_{L1}}R_F + V_{O1} = \frac{V_{O2}}{R_{L2}}R_F + V_{O2}$$

Solving for R_F yields:

$$\left(\frac{V_{O1}}{R_{L1}} - \frac{V_{O2}}{R_{L2}}\right)R_F = V_{O2} - V_{O1}$$

$$R_F = \frac{(V_{O2} - V_{O1})}{\left(\frac{V_{O1}}{R_{L1}} - \frac{V_{O2}}{R_{L2}}\right)}$$

Substituting the values for sample #1 we obtain:

$R_F = 426087\ \Omega$

This was repeated for all five samples and the averages for each frequency were calculated. All calculated impedances are plotted in Figure 6-9. For comparison purposes Figure 6-9 also contains a plot of the theoretical impedance at each test frequency as determined by Equation 5-2. It is evident from Figure 6-9 that all samples exhibited a higher than predicted electrical impedance. This is not to say that all samples would exhibit this higher impedance. However, if these samples were used for the implant they would produce a lower than expected output, possibly offsetting the effects of the larger g_{33} observed in the previous test. This will be discussed in the next chapter.

6.3 VOLTAGE FIELD PATTERN MEASUREMENTS

Nerve fibers can be depolarized if an applied potential field increases the resting potential to the all or none point. In the event that the PVDF film cannot supply sufficient current to depolarize the adjacent auditory nerve fibers the electric field produced by the implant may still produce a potential drop of sufficient magnitude along one or more nerve fibers causing depolarization. It was decided to simulate one of the stimulation sites of the implant and record the potential field patterns outside the electrode.

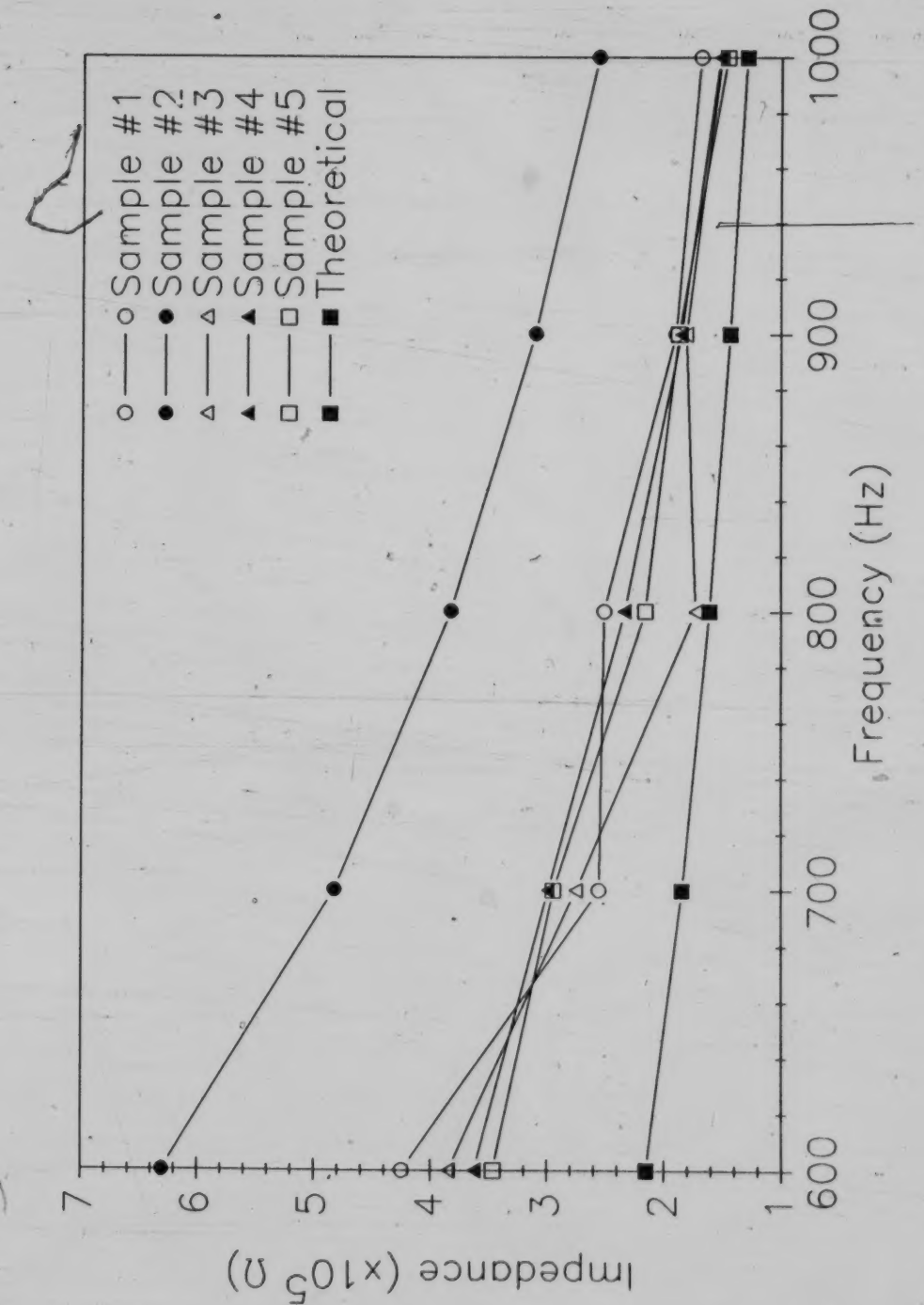

Figure 6-9: Electrical Impedance of Test Samples *vs.* Frequency

In order to record the necessary data the approximate structure of the implant was stimulated with all dimensions increased by a factor of ten. A piece of glass-epoxy circuit board material of thickness 0.85 mm with of the copper foil etched off was used to simulate the insulating properties of the PVDF film. It was cut into a strip 1 cm wide and 13 cm long. This would correspond to actual dimensions of 1 mm x 13 mm x 85 μm. The thickness of the circuit board did not correspond to an actual thickness of 28 μm because a thinner board did not possess the necessary rigidity for this test. This was deemed acceptable since a thinner board would not significantly decrease the length of the path the current from the electrodes would follow.

The electrodes were constructed out of stainless steel strips 70 μm thick. Stainless steel was chosen because of its corrosion resistance. The strips were attached to the top and bottom of the implant board with epoxy. Enameled wire was then attached to each electrode strip to allow connection to a voltage source. Ordinary nail polish was used to paint an electrode pattern on the stainless steel strips. The top electrode consisted of a square area 0.5 cm on a side. The rest of the stainless steel was insulated with nail polish. On the bottom, a strip 0.5 cm wide and running the length of the board was left exposed to create the bottom electrode. Again, nail polish was used to insulate all other surfaces. Figure

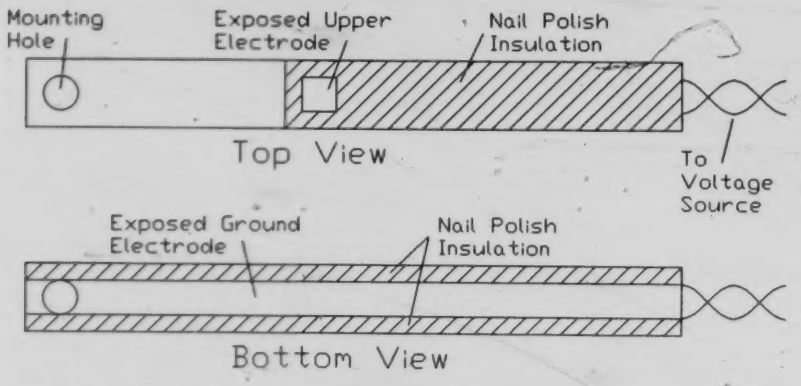

Figure 6-10: Implant Model

6-10 illustrates the implant model.

A platinum electrode was constructed to measure the voltage potentials in the fluid surrounding the implant. A 0.38 mm diameter platinum wire was placed inside a 1.22 mm outer diameter glass capillary tube with a small amount of wire protruding from each end. Epoxy was used to seal the tube. One end of the platinum wire was then sanded flush with the end of the capillary tube to form the electrode surface. The electrode was then attached to a positioning device capable of moving in 10 μm steps in the X and Z directions. Both the positioning device and the implant were mounted on a common base plate as seen in Figure 6-11. This ensured that there would be no relative movement between the two and allowed the measuring electrode to consistently return to the same

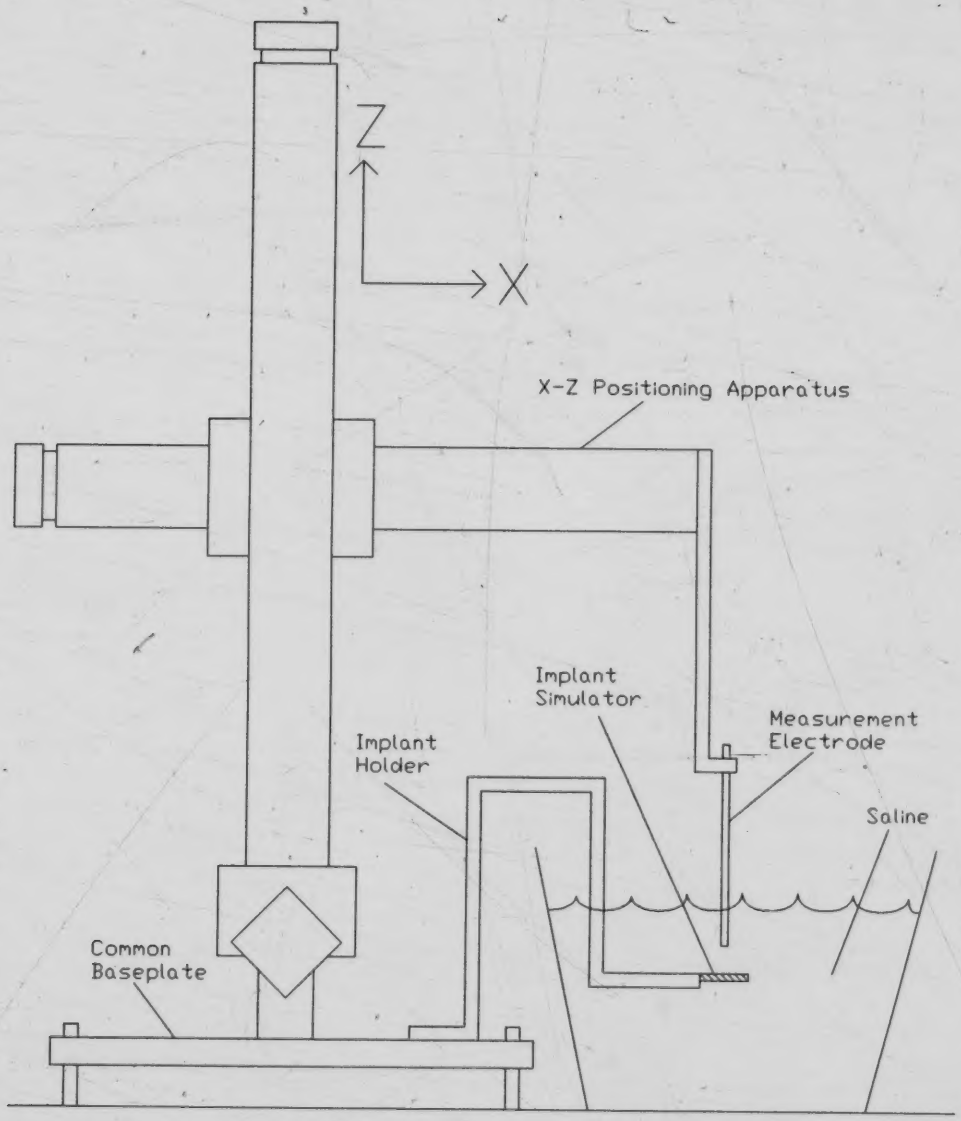

Figure 6-11: Potential Field Measurement Apparatus

starting point for multiple sets of measurements.

The implant and the measuring electrode were immersed in a physiological saline solution since saline is electrically similar to perilymph [11]. The electrode was connected to a high impedance operational amplifier wired as a voltage follower (ie. gain = 1). Due to the extremely high input impedance of this particular op-amp ($10^{12}\Omega$), any negative effects the measurement electrode may have had on the measurements were eliminated. A Beckman HD153 digital multimeter was used to measure the output of the op-amp which corresponded to the potential seen at the tip of the measuring electrode. A 100 mV_{peak} AC signal at 1000 Hz was applied to the top square electrode of the implant. The bottom electrode was grounded and all measurements were made with respect to this electrode.

Due to the symmetry of the upper electrode only the potential field patterns in a plane along the center of the electrode perpendicular to the long axis of the implant were measured (see Figure 6-12). The potentials will be the highest in this plane and the field will be parallel to the nerve fibers we want to stimulate. All measurements were made using a common starting point. This point was chosen so that the side of the measuring electrode was just touching the nail polish insulation surrounding the top electrode and the face of the measuring electrode was making contact with the top

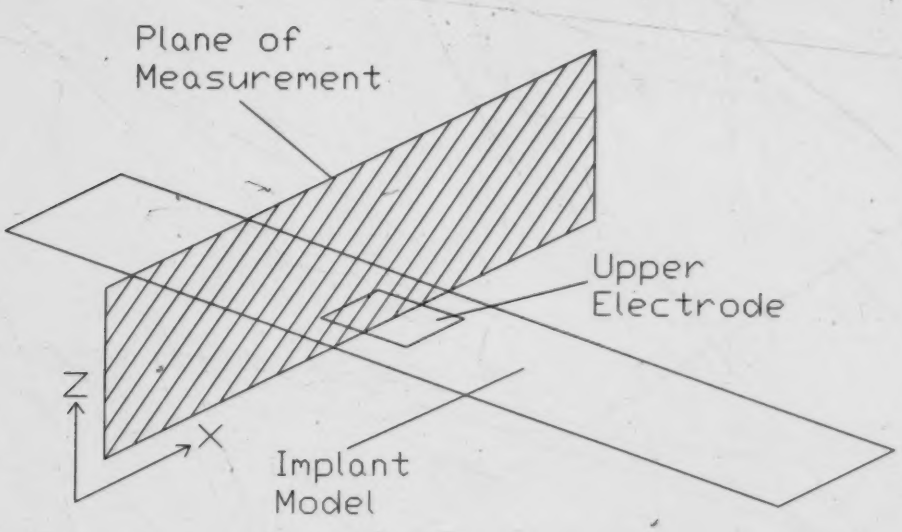

Figure 6-12: Plane of Field Pattern Measurement

electrode. As a result the center of the electrode is 0.61 mm from the edge of the top electrode. The measuring electrode was then moved up and in a positive and negative direction along the measurement plane in order to map the potential patterns. The height above the implant electrode for potential of 90 mV, 80 mV, 70 mV, 60 mV, 50 mV, 40 mV and 30 mV were recorded in steps. The field lines are plotted in Figure 6-13. Referring to the X-axis of Figure 6-13, 0 represents the aforementioned common starting point and -0.61 mm and +4.4 mm are the edges of the top implant electrode. In order to ensure the accuracy of the data the mid-point of each potential line was recorded an additional five times. Between each set of measurements the saline

solution was replaced. The mean values were used in Figure 6-13. The standard deviation of each value was too small to plot. They are listed in Table 6-2 instead.

Table 6-2: Mean and Standard Deviation of Potential Field Accuracy Measurements

Potential (mV)	Mean (mm)	Stand. Dev. (mm)
90	0.745	0.022
80	1.11	0.024
70	1.53	0.024
60	2.03	0.027
50	2.65	0.028
40	3.53	0.028
30	4.92	0.039

Although the field lines produced in this experiment are the result of a 100 mV_{peak} input voltage, the resulting potentials for any input voltage can be extrapolated. The 90 mV field line corresponds to 90% of the input potential, the 80 mV line is 80% and so on. These percentages can be used to determine the field potentials regardless of the input magnitude.

Unfortunately one anomaly did occur in this experiment. As the measuring electrode was moved up from the implant electrode surface to the 90 mV potential line the voltage was observed to first increase before decreasing as expected. The results can be seen in Figure 6-13. The distance between the 80 mV line and the 90 mV line is less than the distance between the 90 mV line and the upper electrode surface. Clearly according

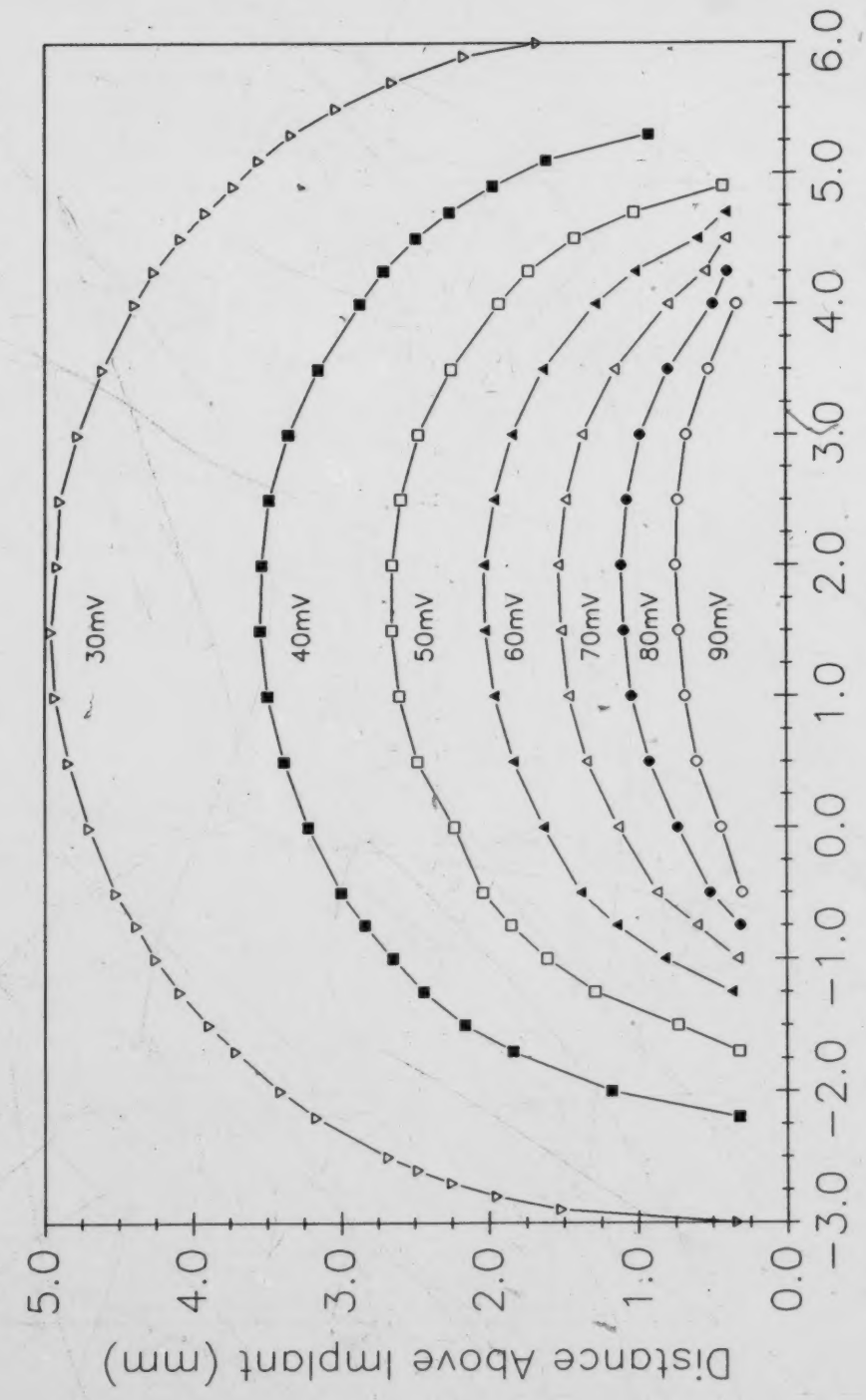

Figure 6-13: Potential Field Around the Implant Model

to electromagnetic [14] and volume conductor theory [15] this should not be so. However at this time no explanation for this result could be found. One hypothesis is that the large diameter of the measuring electrode (1.22 mm) somehow disturbed the potential field close to the upper electrode surface. At greater distances from the stimulating electrode the size of the measuring electrode would have less effect since the field lines are further apart. Another hypothesis is that stray capacitance between the platinum wire in the glass sleeve and the surrounding bath may have disturbed the field. These hypotheses have yet to be proven.

The anomaly in the measurements not withstanding, it is possible to use Figure 6-13 to determine the potential drop between two arbitrary points an arbitrary distance above the electrode as originally intended. In the next chapter we will determine if this potential field will be strong enough to cause stimulation of the auditory nerve.

7. DESIGN REVISIONS

7.1 Electrical Output

The voltage constant test in chapter 6 revealed that it is possible to obtain, (at least for our samples), values of g_{33} up to 4.3 times greater than the manufacturer's specifications (Although it was not tested we will assume that g_{31} also increased by the same amount). Unfortunately the second experiment indicated that the internal impedances of our test samples were greater than the values given by the manufactures. There was no correlation, however, between increased impedance and increased g_{33}. In other words the samples with the higher g_{33} did not necessarily have the higher impedances. When choosing material for the actual implant it would be prudent to consider several samples and choose the one with the best combination of g_{33} and impedance. To do this an arbitrary load could be selected and then the output of each sample could then be calculated. For example let us choose sample #1 with an arbitrary load of 100 kΩ and a stimulating pressure of 5 kPa at 1 kHz:

$$V_{out} = \frac{R_L}{R_L + R_I} V_F \qquad (7\text{-}1)$$

$$= \frac{1 \times 10^5}{1 \times 10^5 + 168262}(0.0591)$$

$$V_{out} = 0.022 \text{ V}$$

Using this same method on the other four samples

indicates that sample #4 has the best overall output characteristics. However, will the output of this sample be sufficient to cause nervous stimulation in the ear? In order to answer this we must first determine the load the film would see if it were inside the ear. As mentioned in chapter 6 the conductivity of perilymph and the tissues surrounding the basilar membrane is very similar to that of saline. The saline bath in the previous chapter acted like a load of 115Ω. This was calculated by measuring the current passing through the test implant and saline and dividing it into the 100 mV input voltage.

The resistance of any material is determined by multiplying its resistivity by its length and dividing by its cross-sectional area. Since all dimensions of our test apparatus were increased by a factor of ten over actual size, the resistance measured in our test bath was one tenth the resistance the actual implant would see. The impedance of the electrodes will also increase because of the smaller geometric area and the fact that a different electrode material may be used. For our calculations we will assume an overall increase in impedance by a factor of ten which means the actual implant would see a load of 1150Ω.

We now have all the necessary information to calculate the output of the actual implant using the material from sample #4. Using equation 4-1, the

pressure values from chapter 5 and the voltage constant data from chapter 6 we can calculate the voltage outputs of implant #1 and implant #2. The film voltage for implant #1 will be 165 mV and it will be 16.49 V for implant #2. The impedance of sample #4 was an average of 44% higher than theory predicted. This translates into 60.42MΩ at 1000 Hz using equation 5-2. For a load of 1150Ω, equation 7-1 can then be used to calculate the output of the two implants to the surrounding media. Implant #1 will have a maximum voltage output of $3.14\mu V_{peak}$ which corresponds to an output current of $2.73nA_{peak}$. The charge delivered to the load at 1000 Hz is $1.37pC_{peak}$/phase. Each period of the 1000 Hz input stimulus contains a positive phase and a negative phase. The units C/phase refer to the amount of charge delivered to the load during each phase of the input stimulus. Repeating the above procedure for implant #2 results in a maximum output voltage of $314\mu V_{peak}$ and a current of $0.273\mu A_{peak}$. The charge delivered to the load at 1000 Hz is $0.136nC_{peak}$/phase. These are only general calculations to determine the approximate output of the implant. They are however, optimistic figures since the working implant may use different electrode materials and will be placed in a medium that will present a larger load than the one used here.

Many auditory implants are currently in use throughout the world [2]. The results obtained with

these implants will allow us to determine if our implant designs will stimulate the auditory nerve. I.J. Hochmair-Desoyer and E.S. Hochmair [14] have designed and tested an eight channel auditory prosthesis. Their normal stimulation regimes use charges of 2 - 60 nC/phase. Loel *et al.* [11] have done threshold studies on the auditory nervous system. Their studies indicate that stimulation charges of 5 - 20 nC/phase are necessary between 300 Hz and 5000 Hz (the range we are interested in). From their auditory prostheses research Eddington *et. al.* [15] have determined that currents of greater that 5μA are necessary to achieve stimulation. This threshold current increases as the distance between electrode and nerve increases [11]. In addition, if nervous damage has resulted in the loss of myelin from the auditory fibers, stimulation thresholds will also increase. When we compare the output of our implant designs with the current values already in use it is clear that our implants do not provide enough current to produce stimulation of the auditory nerve. The output of implant #2 is at least two orders of magnitude too small and the output of implant #1 is four orders of magnitude too small. Since the output impedance of both implants is inversely proportional to frequency, the output impedance will go down as frequency goes up. At a frequency of 20kHz the output of implant #2 would produce the minimum current levels given earlier. Unfortunately,

speech (between humans) does not take place at such high frequencies.

One other method remains to us to obtain excitation of the auditory nerve. Nerve membranes typically have a resting potential of 80 mV (inside negative). If a small area of nerve membrane has its resting potential increased by about 20 mV the nerve will fire.

Figure 6-13 illustrates the potential field surrounding a typical stimulation site on either implant. Using Figure 6-13 we can determine the potentials produced by the implant around any nearby nerve fibers. Since the upper face of the implant rests against the basilar membrane the upper face will be roughly parallel to the auditory nerves. Twenty-five to fifty micrometers above the electrode face (where the nerve fibers are likely to be) and to the left of the "0" point in figure 6-13, the electric field is 0.754 V/m. This means that the field would have to extend along nearly 3 cm of nerve fiber to achieve a voltage drop of 20 mV. Given the dimensions of the cochlea this is clearly not possible.

7.2 OTHER CONSIDERATIONS

Up to this point we have dealt mainly with the electrical aspects of the implant. There are also several mechanical and physiological problems which also must be investigated. These problems are beyond the scope of this thesis. They are presented here as topics for further study.

This prosthesis will not work for all profoundly deaf individuals. It will therefore be necessary to develop a test regime to determine possible candidates. Once these candidates are found testing to determine the locations of surviving afferent nerve populations should be performed. This will allow electrode patterns to be determined for optimal chance of stimulation.

In order to achieve the desired results it is obvious that the implant should have as little affect on the mechanics of the basilar membrane as possible. This would suggest that the implant be placed so that it does not quite touch the basilar membrane. However, maximum excitation will occur when the implant is resting on the basilar membrane. This also puts the implant as close as possible to the auditory nerves which we are trying to stimulate. Regardless of where the implant is situated, its frame cannot rest on the basilar membrane. The basilar membrane supports a small blood vessel and any type of rigid frame resting on this blood vessel would restrict the flow of blood through it possibly damaging the membrane. In addition, the frame would interfere with membrane movement thereby altering the properties of the membrane. The frame itself must be of a corrosion resistant, electrically non-conductive material. In addition the material must retain sufficient rigidity when used on a microscopic scale. This will enable the implant to be made with as small a cross-section as

possible thereby reducing its effect on the flow of perilymph in the cochlea. Since perilymph couples the movement of the stapes to the basilar membrane its movement should not be impeded in any way. A 28 μm thick 1 mm wide piece of PVDF film occupies only 5% of the cross-sectional area of the scala tympani at the apical end and even less as we move towards the basal end. Therefore the greatest restriction of perilymph flow will undoubtedly be caused by the frame which should be made as small as possible.

Since both implant designs should rest against the basilar membrane it is be important to know the long term effects of the implants on the membrane. Both implants will prevent contact between the basilar membrane and perilymph. This holds to a lesser degree in implant #2 because it is in sections. It is necessary to know if this loss of contact will affect the basilar membrane's characteristics in any way. It is also necessary to know if contact between the basilar membrane and the implant (when the are moving) will cause damage to the basilar membrane.

If we are optimistic and assume that no damage or loss of function occurs due to the presence of the implant then the most important question is how will the basilar membrane behave with the implant resting against it? A great deal of research has been done to determine how the cochlea and in particular the basilar membrane

responds to stimuli [37-58]. Once the implant design has been finalized and its mechanical properties determined, these properties can be incorporated into the equations modeling the basilar membrane in the above mentioned works. It should then be possible to determine to a reasonable degree how the basilar membrane-implant combination will perform.

8. ALTERNATE MATERIALS AND METHODS

The original purpose of the paper was to provide a complete design study of a piezoelectric cochlear implant. While the general idea appears sound, the data presented in the last few chapters indicates that the piezoelectric material PVDF will not be able to provide adequate stimulation levels. Therefore, it was decided to investigate different materials that could possibly provide an adequate stimulus and also explore methods of stimulation other than direct stimulation by the piezoelectric material.

8.1 Electrets

The material considered to replace the PVDF film was an electret, and electrical cousin to piezoelectric materials. An electret is a piece of dielectric material with a semi-permanent electrical charge. The charge is semi-permanent in that the time constant for the decay of the charge is much longer than the time over which studies are performed on the electret material. An electret was considered because of the large charge densities possible on the surface of the material. For example, the 1.0mm x 1.0mm x 28μm thick piece of PVDF film in implant #2 produced a no load voltage of 165mV when subject to a pressure of 3990 Pa. This corresponds to a surface charge density of approximately 9×10^{-9} C/cm^2. For a 10 μm thick teflon electret, it is

possible to obtain charge densities of up to 1×10^{-7} C/cm^2 [17].

The electret has seen widespread use as a transducer. One of the more well know types of these transducers is the electret microphone. A structure similar to the microphone is considered for the cochlear implant and is illustrated in Figure 8-1. An electret of

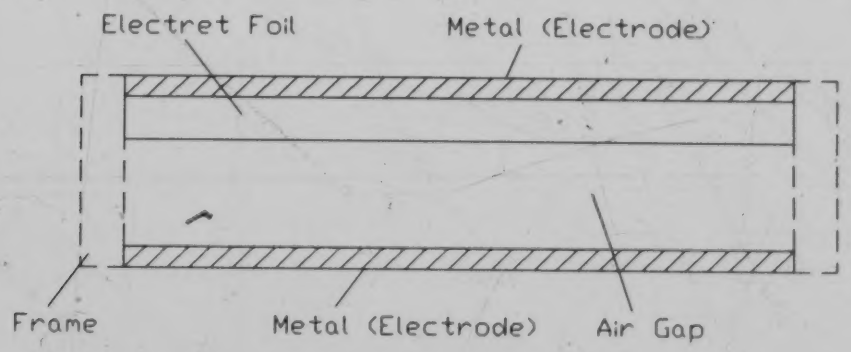

Figure 8-1: Electret Transducer

thickness S with one metallized side is held a distance D above a metallized back electrode. When sound waves, or any form of pressure, impinge on the electret foil, the electret moves an amount ΔD. This causes a change in the transducer's capacitance which results in an output voltage. Sessler et. al. [16] has shown that for a microphone with uniform properties the output voltage is given by:

$$V = \frac{S\sigma\Delta D}{\varepsilon_o(S + \varepsilon D)} \qquad (8\text{-}1)$$

Where: ε_o = permittivity of air

ε = dielectric constant of the electret

σ = charge density on the unmetallized surface of the electret

If R in Figure 8-1 is finite then the output of the microphone becomes:

$$V_o = \frac{V\omega RC}{\sqrt{1 + (\omega RC)^2}} \qquad (8\text{-}2)$$

where C is the capacitance of the transducer. Sessler has also shown that the capacitance of a microphone with uniform properties is:

$$C = \frac{\varepsilon\varepsilon_o A}{(S + \varepsilon D)} \qquad (8\text{-}3)$$

where A is the area of the electret membrane.

Let us consider the 10 μm thick teflon electret mentioned earlier with a charge density of 1×10^{-7} C/cm^2 on its unmetallized surface in a structure like that in Figure 8-1. The electrode area A is 1×10^{-6} mm^2 (the same as the piezo film in chapter 5). The air gap thickness D is chosen to be 35 μm and the dielectric constant of teflon is 1.2 Assume when the basilar membrane deflects downwards the change in the air gap thickness is 30 μm. The resulting no load voltage is:

$$V = \frac{S\sigma\Delta D}{\varepsilon_o(S + \varepsilon D)}$$

$$V = \frac{(10 \times 10^{-6})(1 \times 10^{-3})(30 \times 10^{-6})}{(8.85 \times 10^{-12})(10 \times 10^{-6} + 1.2(35 \times 10^{-6}))}$$

$$V = 651.89 \text{ V}$$

When the electret foil has deflected down the air gap is only 5 μm. This results in a capacitance of:

$$C = \frac{\varepsilon\varepsilon_o A}{(S + \varepsilon D)}$$

$$C = \frac{(1.2)(8.85 \times 10^{-12})(1 \times 10^{-6})}{(10 \times 10^{-6} + 1.2(5 \times 10^{-6}))}$$

$$C = 0.664 \text{ pF}$$

For our calculations we will use a value for R of 1150Ω, the same value used in chapter 7. For a frequency of 1000 Hz we now use equation 8-2 to determine the output of the electret transducer:

$$V_o = \frac{(651.89)2\pi(1000)(1150)(0.664 \times 10^{-12})}{\sqrt{(1 + (2\pi(1000)(1150)(0.664 \times 10^{-12}))^2}}$$

$$V_o = 3.13 \text{ mV}$$

This voltage corresponds to a current of 2.72 μA. At 1000 Hz the charge delivered to the load is 1.36 nC/phase. According to the sources listed in chapter 7 the charge output of the electret transducer is approximately half the minimum level of charge needed to produce stimulation of the auditory nerve. This is a considerable improvement over the piezoelectric implants we have considered so far.By reducing the size of the air gap and using a thicker electret with a higher charge density it should be possible to achieve stimulation of nearby nerve fibers.

The electret transducer is not without its problems however. Perhaps the biggest problem is the structure of the transducer. Manufacturing it on the microscopic scale we are using will undoubtedly be difficult. In addition the cross-sectional area of the transducer is much greater than the piezoelectric transducers considered earlier. This may adversely affect the

movement of perilymph in the scala tympani thereby impairing the operation of the cochlea. These difficulties not withstanding, at this time the electret transducer seems to show greater promise than the PVDF piezoelectric transducer discussed earlier.

8.2 Alternate Methods

Although electrets seem to show more promise than piezoelectrics we are not about to totally abandon them. It is clear that until material science produces piezoelectric materials with voltage constants much larger than those currently available, we must augment the output of our piezoelectric transducer is some way. This will entail adding an amplifier, power supply and stimulating electrodes to our transducer. Considering the small size of our target location the logical choice for the amplifier would be an integrated circuit FET amplifier with its low power dissipation and high input impedance. IC technology has been used to create a number of sensors and transducers for biomedical research [18]. It should be possible to adapt their results for our purposes. In fact one researcher has already built a constant current source for nerve stimulation using CMOS and hybrid technology [19].

Of course all these devices need some sort of power source. The method of choice is a transdermal RF link where RF energy is transmitted through the skin, rectified and used to power an implant. RF coupling to

millimeter and sub-millimeter size power sources has also been investigated [20]. Implantable batteries are another possibility that bears consideration.

As with the two other transducers presented already the amplified piezoelectric transducer should alter cochlear mechanics as little as possible. Careful consideration must therefore be given to the placement of the transducer, amplifier circuitry and the stimulating electrodes.

9. CONCLUSIONS

In this thesis the concept of a piezoelectric cochlear implant has been presented. Two possible implant configurations were discussed using PolyVinyliDene Fluoride as the transducer. At this time PVDF is the material of choice because of its corrosion resistance, high voltage constants and high compliance coupled with mechanical strength. Five samples of PVDF were tested to determine the values of their g_{33} voltage constants and electrical impedance. Both properties were found to exceed the manufacturer's specifications. This led to the conclusion that many samples should be tested for use in the implant. The sample that produced the best output (see selection method in chapter 7) would be chosen for use in the implant. Unfortunately both implant configurations produced current outputs that were 2 - 4 orders of magnitude smaller than the levels needed to produce stimulation. These designs and results are based on many assumptions and should in no way be considered the last word in the matter. If a piezoelectric material with a greater g_{33} (increased voltage output) or larger dielectric constant (decreased electrical impedance) is found it can be used in the implant with improved results. Innovations in the design of the transducer may produce superior performance. Thicker films will produce greater outputs. The films

can also be laminated in series or parallel. A parallel configuration would serve to decrease the output impedance.

Alternate materials and methods were also considered. At this time electrets seem to show the greatest promise. The output of the design discussed in chapter 8 fell just short of the minimum level needed to achieve stimulation. Modifications to this design or use of electret films with higher charge densities should improve the results.

Since the output of the piezoelectric film was too small to cause stimulation, amplification of its output was considered. The use of integrated circuit technology to produce extremely small implantable devices and the sources to power them is growing every day. If it becomes evident that piezoelectric films will not soon be able to produce currents of sufficient magnitude to cause stimulation of the cochlear nerve then this implantable technology may become necessary.

As it was mentioned earlier this thesis is based on many assumptions. There are several areas that need investigating. A thorough search should be done for any new piezoelectric materials that exhibit better properties than PVDF. It is necessary to have a thorough understanding of the pressures inside the human cochlea and how the basilar membrane responds to these pressures. Once a better understanding exists of how the

basilar membrane operates, the way in which the membrane-implant combination behaves can be determined.

Regardless of these problems the potential of the piezoelectric cochlear implant is too great to ignore. It offers the possibility of restoring hearing function in profoundly deaf individuals. This simple implant made of strong and reliable materials plus an external hearing aid would be the only components needed. Add to this that the manufacturer of the samples we tested anticipates improvements in piezoelectric film technology and it is clear that a PVDF cochlear implant is deserving of further study.

REFERENCES

1. Yin, Lillian and Segerson, David A., "Cochlear Implants: Overview of Safety and Effectiveness", Otolaryngologic Clinics of North America, Vol. 19, pp. 423-433, 1986.

2. White, R.L., "Review of Current Status of Cochlear Prostheses", IEEE Trans. Biomed. Eng., Vol. 29, pp. 233 -238,1980.

3. Deutsch, Lawrence J. and Richards, Alan M., "Elementary Hearing Science", University Park Press, 1979.

4. Gayakwad, Ramakant A., "Op-Amps and Linear Integrated Circuit Technology", Prentice-Hall Inc., New Jersey, 1983.

5. Deutsh, Sid and Micheli-Tzanakou, Evangelia, "Neuroelectric Systems", New York University Press, New York, 1987.

6. Peterson, L.C. and Bogert, B.P., "A Dynamical Theory of the Cochlea", J. Acoust. Soc. Am., Vol. 22, pp. 396 -381, 1950.

7. Dancer, A. and Franke, R., "Intracochlear Pressure Measurements in Guinea Pigs", Hearing Research, Vol. 2, pp. 191-205, 1980.

8. Nedzelnitsky, V., "Sound Pressures in the Basal Turn of the Cat Coshlea", J. Acoust. Soc. Am., Vol. 68, pp. 1676-1689, 1980.

9. Timoshenko, S. and Woinowsky-Krieger, S., "Theory of Plates and Shells", McGraw Hill Book Co., Inc., New York 2nd Edition, 1959.

10. Altschuler, R.A., Bobbin, R.P. and Hoffman, D.W., "Neurobiology of Hearing-The Cochlea", Raven Press, New York, 1986.

11. Loeb, Gerald E., White, Mark W. and Jenkins, William M., "Biophysical Considerations in Electrical Stimulation of the Auditory Nervous System", Ann. N.Y. Acad. Sci., Vol. 405, pp. 123-136, 1983.

12. Pennwalt Corporation, " KYNAR Piezo Film Technical Manual", Pennwalt Corp.

13. Pickles James O., "The Physiology of the Cochlea", *In* Cochlear Implants. R. F. Grey, Ed., College-Hill Press, Inc., San Diego, 1985, pp. 27-49.

14. Hochmair-Desoyer, I.J., and Hochmair, E.W., "An Eight Channel Scala Tympani Electrode for Auditory Prosthesis", IEEE Trans. Biomed. Eng., Vol. 27, pp. 44 -50, 1980.

15. Eddington,D.K.,Dobelle, W.H., Mladejovsky, M.G., Brackmann, D.E. and Parkin, J.L., "Auditory Prostheses Research with Multiple Channel Intracochlear Stimulation in Man", Ann. Otol. Rhinol. Laryngol., Vol. 87(53), pp. 5-30, 1978.

16. Sessler G.M., and West, J.E., "Foil-Electret Microphones", J. Acoust. Soc. Am., Vol. 40, pp. 1433 -1440, 1966.

17. Sessler G.M., "Physical Principles of Electrets", *In* Topics inApplied Physics: Electrets, Vol. 33, G.M. Sessler Ed., Springer-Verlag, Heidelberg, 2nd ed., pp. 13-80, 1987.

18. Ko, Wen H., "Solid-State Physical Transducers for Biomedical Research", IEEE Trans. Biomed. Eng., Vol 33, pp. 153-162, 1986.

19. Hochmair, Erwin S., "An Implantable Current Source for Electrical Nerve Stimulation", IEEE Trans. Biomed. Eng., Vol. 27, pp. 278-280, 1980.

20. Heetderks, William J.,"RF Powering of Millimerter- and Submillimeter-Sized Neural Prosthetic Implants", IEEE Trans. Biomed. Eng., Vol. 35, pp. 323-327, 1988.

21. BeMent, Spencer L. *et. al.*, "Solid-State Electrodes for Multichannel Multiplexed Intracortical Neuronal Recording", IEEE Trans. Biomed. Eng., Vol. 33, pp. 230 -241, 1986.

22 Smith, R.L. and Scott, D.C., "An Integrated Sensor for Electrochemical Measurements", IEEE Trans. Biomed. Eng., Vol. 33, pp. 83-90, 1986.

23. Crago, Patrick E. *et. al.*, "Sensors for Use With Functional Neuromuscular Stimulation", IEEE Trans. Biomed. Eng., Vol. 33, pp. 256-268, 1986.

24. Galbraith Douglas C. *et. al.*, "A Wide-Band Efficient Inductive Transdermal Power and Data Link with Coupling Insensitive Gain", IEEE Trans. Biomed. Eng., Vol. 34, pp. 265-275, 1987.

25. Soma,Mani *et. al.*, "Radio-Frequency Coils in Implantable Devices: Misalignment Analysis and Design Procedure", IEEE Trans. Biomed. Eng., Vol. 34, pp. 276 -282, 1987.

26. Smith, Michael J.S. *et. al.*, "Analysis, Design and Performance of a Capacitive Pressure Sensor IC", IEEE Trans. Biomed. Eng., Vol. 33, pp. 163-174, 1986.

27. Edell, David J., "A Peripheral Nerve Information Transducer for Amputees: Long-Term Multichannel Recordings from Rabbit Peripheral Nerves", IEEE Trans. Biomed. Eng., Vol. 33, pp. 203-214, 1986.

28. Bowman, Lyn and Meindl, D., "The Packaging of Implantable Integrated Sensors", IEEE Trans. Biomed. Eng., Vol. 33, pp. 248-255, 1986.

29. Prohaska, Otto J. *et. al.*, "Thin-Film Multiple Electrode Probes: Possibilities and Limitations", IEEE Trans. Biomed. Eng., Vol. 33, pp. 223-229, 1986.

30. Busch-Vishniac, I.J. *et. al.*, "A New Approach to Transducer Design Applied to a Foil Electret Acoustic Antenna", J. Acoust. Soc. Am., Vol. 76, pp. 1609-1616, 1984.

31. Voorthuyzen, J. A. and Bergveld, P., "Theoretical Considerations in the Design of Integrated Semiconductor Sensors Applying Electrets", IEEE Trans. Electron Devices, Vol. 32, pp. 1185-1190, 1985.

32. Iovine, John, "Piezoelectric Plastic Film", Radio Electronics

33. Aronson, Robert B., "Rediscovering Piezoelectrics", Machine Design, June 21, 1984, pp. 73-77.

34. Flanagan, James L., "Computational Model For Basilar Membrane Displacement", J. Acoust. Soc. Am., Vol. 34, pp. 1370-1376, 1962.

35. v. Békésy, G., "On The Elasticity of the Cochlear Partition", J. Acoust. Soc. Am., Vol. 20, pp. 227-241, 1948.

36. Bateman, Hugh E., and Mason, Robert M., "Applied Anatomy and Physiology of the Speech and Hearing Mechanism", Charles C. Thomas, Pub., Springfield, Il., 1984, p. 438.

37. Neely,S.T. and Kim, D.O., "A Model for Active Elements in Cochlear Biomechanics", J. Acoust. Soc. Am., Vol. 79, pp. 1472-1480, 1986.

38. Schroeder, Manfred R., "Models of Hearing", Proceedings of the IEEE, Vol. 63 (9), pp. 1332 - 1350, 1975.

39. Holmes, Mark H. and Cole, Julian D., "Cochlear Mechanics: Analysis fo a Pure Tone", J. Acoust. Soc. Am., Vol. 76 (3), pp. 767-778, 1984.

40. Lesser, M.B. and Berkley, D.A., "Fluid Mechanics of the Cochlea. Part 1", J. Fluid Mech., Vol. 51 (3), pp. 497-512, 1972.

41. Neely, Stephan T., "Finite Difference Solution of a Two-Dimensional Mathematical Model of the Cochlea", J. Acoust. Soc. Am., Vol. 69(5), pp. 1386-1393, 1981.

42. Allen, J.B., Sondhi, M.M., "Cochlear Macromechanics: Time Domain Solutions", J. Acoust. Soc. Am., Vol. 66(1),pp. 123-132, 1979.

43. Rhode, Willian S., "Observations of the Vibration of the Basilar Membrane in Squirrel Monkeys using the Mössbauer Technique", J. Acoust. Soc. Am., Vol. 49(4), pp. 1218-1231, 1971.

44. Sondhi, Man Mohan, "Method for Computing Motion in a Two-Dimensional Cochlear Model", J. Acoust. Soc. Am., Vol. 63(5), pp. 1468-1477, 1978.

45. Miller, Christine. E., "Structural Implications of Basilar Membrane Compliance Measurements", J. Acoust. Soc. Am., Vol. 77(4), pp. 1465-1474, 1985.

46. Zweig, G., Lipes, R. and Pierce, J.R., "The Cochlear Compromise", J. Acoust. Soc. Am., Vol. 59(4), pp.975-982, 1976.

47. Viergever, Max A., "Coshlear Macromechanics - A Review",

48. Steele, C.R., "Behavior of the Basilar Membrane With Pure-Tone Excitation", J. Acoust. Soc. Am., Vol. 55(1), pp. 148-162, 1974.

49. Allen, J.B., "Cochlear Micromechanics - A Physical Model of Transduction", J. Acoust. Soc. Am., Vol. 68(6), pp. 1660-1670, 1980.

50. Zwislocki, J., "Theory of the Acoustical Action of the Cochlea", J. Acoust. Soc. Am., Vol. 22(6), pp. 778-784, 1950.

51. Viergever, Max A., "Basilar Membrane Motion in a Spiral-Shaped Cochlea", J. Acoust. Soc. Am., Vol. 64(4), pp. 1048-1053, 1978.

52. Steele, C.R., Taber, L.A., "Comparison of WKB Calculation and Experimental Results for Three-Dimensional Cochlear Models", J. Acoust. Soc. Am., Vol. 65(4), pp. 1007-1018, 1979.

53. Allen, J.B., "Two-Dimensional Cochlear Fluid Model: New Results", J. Acoust. Soc. Am., Vol. 61(1), pp. 110-119, 1977.

54. Steele, C.R., Zais, J.G., "Effect of Coiling in a Cochlear Model", J. Acoust. Soc. Am., Vol. 77(5), pp. 1849-1852, 1985.

55. Keller, J.B., "Asymptotic Analysis of a Viscous Cochlear Model", J. Acoust. Soc. Am., Vol. 77(6), pp. 2107-2110, 1985.

56. de Boer, E. and van Bienema, E., "Solving Cochlear Mechanics Problems With Higher-Order Differential Equations", J. Acoust. Soc. Am., Vol. 72(5), pp. 1427-1434, 1982.

57. Steele, C.R. and Taber, L.A., "Comparison of WKB and Finite Difference Calculations for a Two-Dimensional Cochlear Model", J. Acoust. Soc. Am., Vol. 65(4), pp. 1001-1006, 1979.

58. de Boer, E., "Short Waves in Tree-Dimensional Cochlea Models: Solution for a 'Block' Model", Hearing Research, Vol. 4, pp. 53-57, 1981.

APPENDIX I

As mentioned in the main body of this paper the PVDF film was modeled as a thin square membrane. The methods of Timoshenko and Woinowsky-Krieger are used to calculate the membrane stresses inside the membrane. Notation will be defined first:

V = Strain energy

E = Modulus of elasticity in tension and compresion
$= 3 \times 10^{9} N/m^{2}$

h = Thickness of the membrane
$= 28 \times 10^{-6}$ m

a = Length of one half of one side
$= 0.25$ mm

w_o = Displacement of the center of the membrane

q = Load pressure on the film

ν = Poisson's ratio

MEMBRANE MODEL

The plate is considered as a square membrane with sides of length $2a$ subject to a uniform load (See Figure A-1). Satifying the condition that displacement must vanish at the boundry, the strain energy for $\nu = 0.25$ is given by:

$$V = \frac{Eh}{7.5}\left[\frac{5\pi^4 w_o^4}{64a^4} - \frac{17\pi^2 c w_o^2}{6a} + c^2\left(\frac{35\pi^2}{4} + \frac{80}{9}\right)\right] \qquad (a)$$

The principal of virtual displacements gives :

$$\frac{\partial V}{\partial c} = 0 \qquad (b)$$

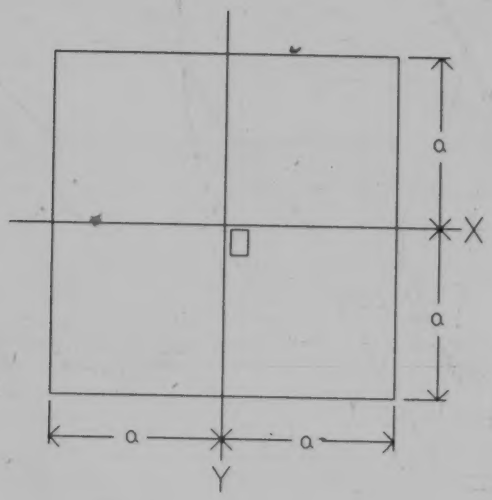

Figure A-1: A Square Membrane With Sides of Length 2a.

$$\frac{\partial V}{\partial w_o}\delta w_o = \int_{-a}^{+a}\int_{-a}^{+a} q\ \delta w_o \cos\frac{\pi x}{2a} \cos\frac{\pi y}{2a}\, dxdy \qquad (c)$$

Substituting (a) for V, we obtain using (b):

$$c = 0.417\frac{w_o^2}{a}$$

and from (c):

$$w_o = 0.802a \sqrt[3]{\frac{qa}{Eh}} \qquad (d)$$

the corresponding tensile membrane stress is:

$$\sigma = 0.396 \sqrt[3]{\frac{q^2Ea^2}{h^2}} \qquad (e)$$

For a distributed load of 3990 Pa:

$$\sigma = 0.396 \sqrt[3]{\frac{(3990)^2 (3 \times 10^9)(0.00025)^2}{(28 \times 10^{-6})^2}}$$

$$\sigma = 618.4 \text{ kPa}$$